RIVISTA DEL NUOVO CIMENTO VOL. 6, N. 10 1983

Multiplicities, p_T Distributions and the Expected Hadron → Quark-Gluon Phase Transition.

R. HAGEDORN

CERN - Geneva, Switzerland

(ricevuto il 5 Gennaio 1984)

Dedicated to Prof. Bruno Ferretti
on the occasion of his seventieth birthday

1. – Introduction.

In the last few years a large amount of theoretical work, using the most varied methods and arguments, has led to the now common belief that a —presumably first order—phase transition from hadrons to a quark-gluon plasma takes place at a transition temperature of 0.150 to 0.200 GeV and at densities not much larger than in nuclei. This holds for hadron matter with total baryon number and strangeness zero; if these are not zero and their conservation is enforced by chemical potentials, the transition temperature will depend on the latter. This case, however, will not interest us here.

Presently the only available theoretical models starting from first principles (QCD Lagrangian) are QCD lattice calculations, a sort of experimental theory. They definitely seem to establish the existence of a phase transition. The main point is, however, that all other models lead to the same qualitative—and in most cases even quantitative—results. Therefore, if one wishes to confront the current theoretical ideas with experiments, one might choose among the various models any one which has a sufficient number of explicitly calculable predictions. We choose the statistical-bootstrap model (SBM).

All approaches suffer in one way or another from the idealizations necessary to enable theorists to arrive at any results at all: in the SBM the main idealizations are the assumptions of *equilibrium* in *infinitely* extended matter, both very far from the real situation in particle collisions (and even in heavy-ion collisions).

The number of papers directly and indirectly concerned with the phase transition at hand is so large that it would be impossible to give a list of references doing justice to all authors. Instead I refer to the Bielefeld « International Symposioum on Statistical Mechanics of Quarks and Hadrons » (1980) [1] and to the Bielefeld Workshop « Quark Matter Formation and Heavy-Ion Collisions » (1982) [2] where all present ideas and all relevant references are available. In the course of this paper I shall then refer only to works tightly connected with the presentation; my apologies go to all authors who might feel they should have been quoted but who have not.

1·1. *The experimental facts.*

Remark. We shall, in the main body of this paper, assume that the « measured $\langle p_T \rangle$ *» are indeed the true* $\langle p_T \rangle$*, although there can be serious doubts about this (to be explained in appendix B). For our purpose the qualitative trends are more important than the exact numerical values.*

Figure 1.1 is taken from ref. [3] and exhibits several important points:

i) $\langle p_T \rangle$ increases with the multiplicity per unit rapidity dN/dy,

ii) at higher multiplicites it levels off.

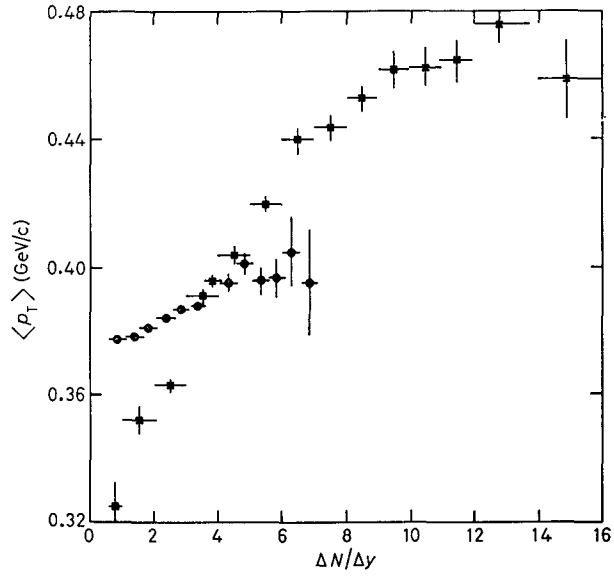

Fig. 1.1. – The average transverse momentum as a function of charged-particle density in the central rapidity region of proton-antiproton collisions at ISR and CERN $p\bar{p}$ collider energies: • ISR proton-proton, $\sqrt{s} = 63$ GeV, $|Y| < 2.0$; ▪ CERN collider, proton-antiproton, $\sqrt{s} = 540$ GeV, $|Y| < 2.5$. (Figure taken from ref. [3].)

We shall take these two qualitative statements for granted. Two other features seem rather to indicate that the quantitative values of $\langle p_T \rangle$ might still contain some systematic errors:

iii) the multiplicity dependence of $\langle p_T \rangle$ at ISR has been observed only very recently [3*a*], while before in measurements with larger errors it seemed to be absent [3*b*, *c*];

iv) the $\langle p_T \rangle$ at low multiplicities at ISR lie *above* those of the collider; this is ulikely to be true.

In fact, as pointed out in appendix B, the $\langle p_T \rangle$ values may depend appreciably on extrapolation methods used when the p_T distribution is measured over an interval with a lower cut. The remaining differences at low multiplicities (between ISR and collider) are of the order of the errors discussed in appendix B and suggest that we should presently not worry about point iv) above.

Figure 1.2 from ref. [4] shows that the p_T distributions at the collider differ for different multiplicities over the whole range of measured p_T and that the effect on $\langle p_T \rangle$ is not so much due to the large p_T tails ($\geqslant 2$ GeV/c) which contribute only a small fraction of the measured particles, but must come essentially from lower p_T where the usual thermodynamic interpretation (Boltzmann spectrum) implies then an apparent change of temperature with multiplicity.

Figure 1.3 from ref. [4] shows the overall p_T distribution with its « thermo-

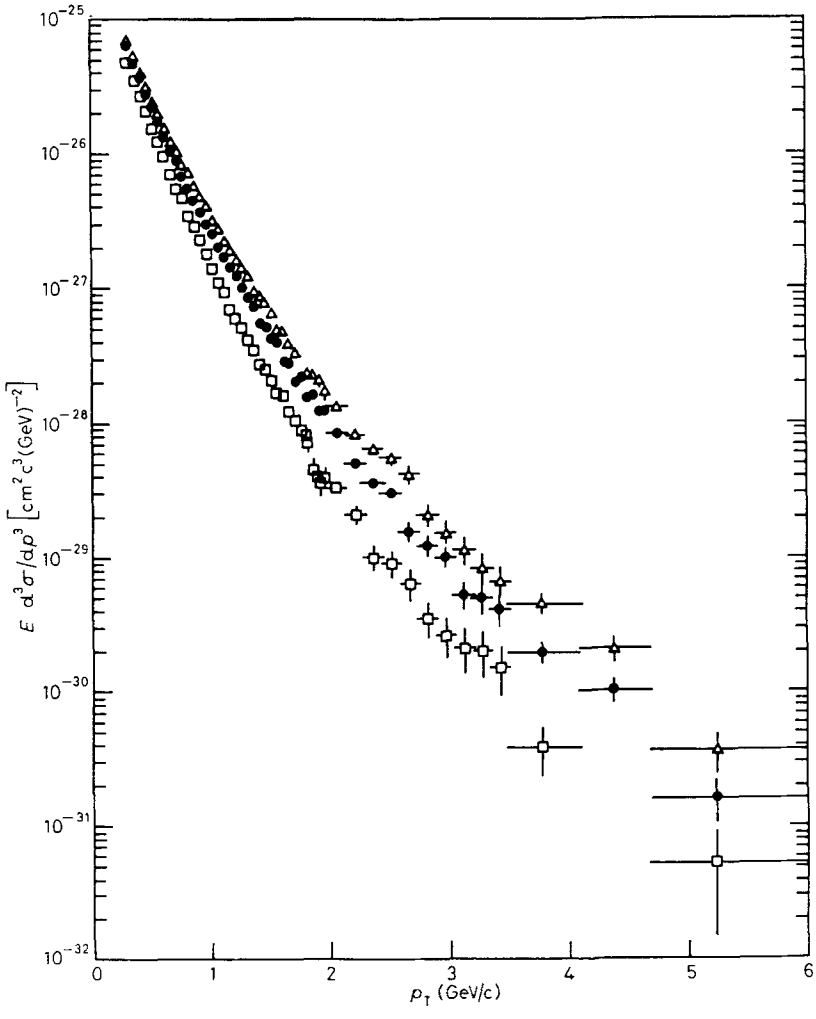

Fig. 1.2. – Transverse-momentum distribution for different multiplicities at $\sqrt{s} = 540$ GeV. The slope rises with multiplicity already at rather low ($\geqslant 1$ GeV/c) p_T. $\triangle$ $\langle n/\Delta y\rangle = 10.2$, $\bullet$ $\langle n/\Delta y\rangle = 5.7$, $\square$ $\langle n/\Delta y\rangle = 2.4$. (Figure taken from ref. [4].)

dynamic » low-p_T part and the typical large-p_T tail (already seen at ISR), which we shall interpret as probing the quark-gluon plasma. The fit [4] to the data is with a QCD-inspired formula discussed in appendix B, where it is shown that, in spite of its looking impressive here, it is unsuitable for determining $\langle p_T\rangle$.

1·2. *The theoretical model.* – Our interpretation of the data will be done in the framework of a recent version of the statistical-bookstrap model (SBM), developed in collaboration with J. RAFELSKI. We shall present here only results and refer for their derivations to the original papers [5-8].

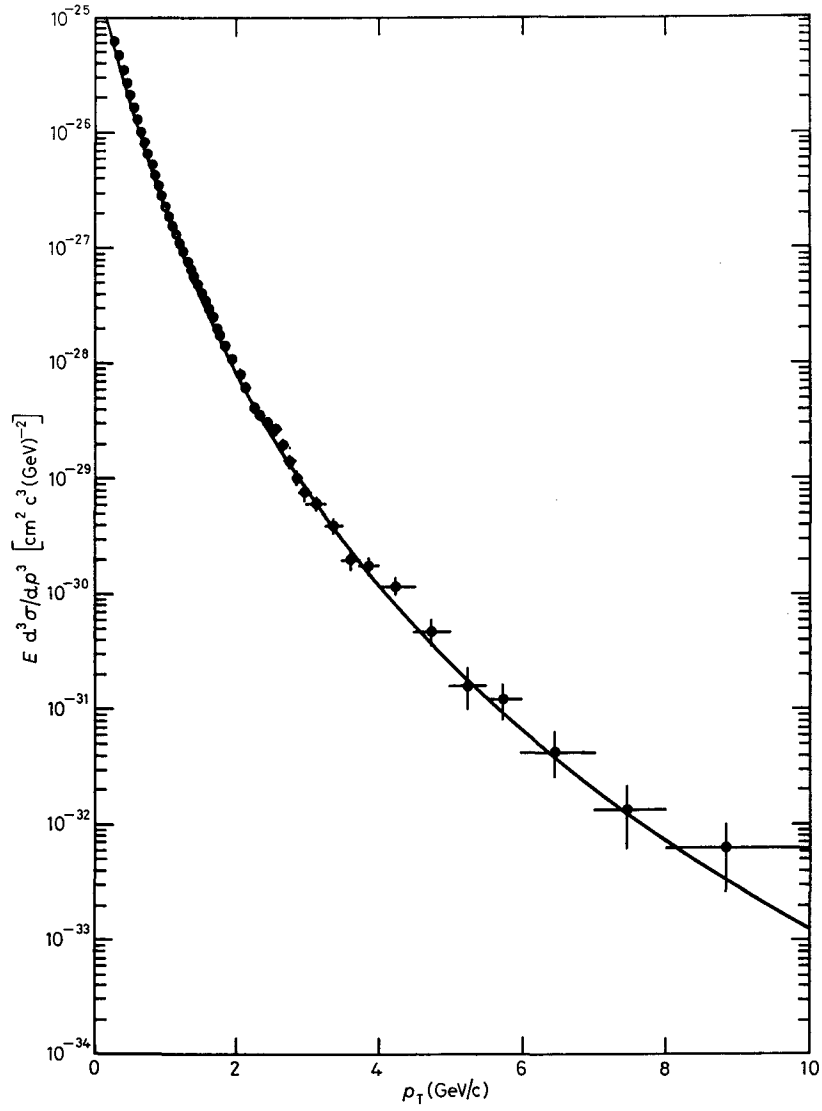

Fig. 1.3. – Inclusive p_T distribution at $\sqrt{s} = 540$ GeV fitted by a semi-empirical formula discussed in appendix B. • $(h^+ + h^-)/2$, $|y| < 2.5$ UA1. (Figure taken from ref. [4].)

The model considers a strongly interacting hadron gas; attractive interactions are represented by allowing all possible hadron reactions A + B + + ... $\rightleftarrows$ A′ + B′ + ... compatible with four-momentum and baryon number conservation (other conservation laws can be added); the possible types of particles A, B, ... form the *hadronic mass spectrum* $\tau(m^2, b)$ which plays a central role in the model: $\tau(m^2, b)\,\mathrm{d}m^2$ is the number of different types of hadrons with baryon number b and mass in $\{m^2, \mathrm{d}m^2\}$. To $\tau(m^2, b)$ belong the « input

particles » pion and nucleon (strange, charmed ... particles may be added but are here not important) as well as *all* allowed bound and resonant states and *all* corresponding antiparticles. It has been shown that, if *all possible* particles {A, B, ...} are counted in $\tau(m^2, b)$, the interacting-hadron gas formally reduces to a mixture of infinitely many ideal gases with mass spectrum $\tau(m^2, b)$. Applying this same idea also to its constituents, clusters of mesons and baryons, one is led to consider these too as systems of strongly interacting constituents, hence again as a mixture of ideal gases with mass spectrum $\tau(m^2, b)$—thus the clusters counted in $\tau(m^2, b)$ consist of clusters, which consist of clusters, etc. This self-consistency requirement generates an (infinitely) nonlinear integral equation (*) for $\tau(m^2, b)$, which has a *unique* physical solution growing exponentially in m:

$$\tau(m^2, b) = f(m^2, b) \exp\left[m/T_c(b)\right], \tag{1.1}$$

where $f(m^2, b)$ is polynomially bounded; $T_c(b)$ is calculable from the bootstrap equation. In thermodynamics $\tau(m^2, b)$ appears in integrals of the type

$$\int_{m_0}^{\infty} \mathrm{d}m^2 \int_{m}^{\infty} \mathrm{d}E\, g(m, E, b, \ldots) \exp\left[-E/T\right] \tau(m^2, b) = \tag{1.2}$$

$$= \int_{m_0}^{\infty} \mathrm{d}m^2 \int_{m}^{\infty} \mathrm{d}E\, h(m, E, b, \ldots) \exp\left[-\frac{\sqrt{p^2 + m^2}}{T} + \frac{m}{T_c(b)}\right]$$

which do not exist for $T > T_c(b)$. Since thermodynamic quantities (energy density, particle number and baryon number densities, etc.) are represented by such integrals, *they have some singularity at $T_c(b)$ indicating a phase transition.*

Calculations simplify if one does not require strict, but only average baryon conservation (other conservation laws can be included) by introducing a baryon chemical potential μ; then the critical temperature is $T_c(\mu)$.

This settles the attractive forces. Repulsive forces are dealt with *à la* Van der Waals by giving each particle a volume, from which other particles are excluded. Introducing this concept in the BE, leads automatically to the result that the proper volume of a particle must be proportional to its mass [9], a feature which SBM shares with the bag model [10] and with nuclear physics. If now thermodynamics is, in addition to the exponential mass spectrum, equipped also with finite (mass-proportional) particle volumes, the singularities due to $\tau(m^2, \mu)$ are somewhat weakened (quantities which diverge at $T_c(\mu)$ for point particles diverge less or may even become finite for extended particles), but they remain at the same place in the (T, μ)-plane. We have then the following situation depicted in fig. 1.4.

(*) The « bootstrap equation » (BE) of the form τ = input particles $+ \sum_{2}^{\infty} \int \ldots \int$ {products of δ-functions and τ's}.

Inside the region called « hadronic phase » we have a gas consisting of all sorts of hadron clusters; the nearer we come to the critical curve, the more clusters coalesce into ever bigger clusters and, when we reach the critical curve, they all disappear in one infinitely large cluster of infinite mass—in striking similarity to condensation where droplets coalesce in larger droplets and finally into the liquid phase. As the volume of a cluster is proportional to its mass, all clusters have the same energy density ε_0 and on the critical curve the whole system has then reached this density ε_0.

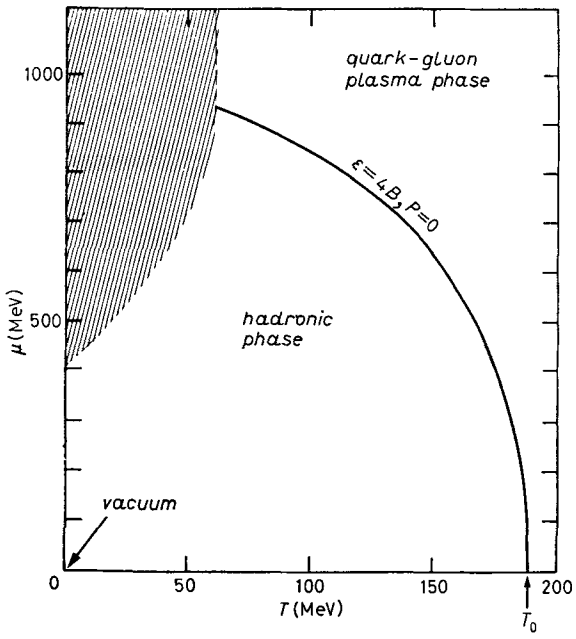

Fig. 1.4. – The singular curve of the statistical-bootstrap model [5]. In the shaded region the model is unreliable, because there the (otherwise negligible) effects of Bose-Einstein and Fermi-Dirac statistics become important.

We now relate SBM to the bag model. The two models share the mass-volume relation, which in the bag model is written $M = 4B \cdot V$. It is reasonable to take the SBM mass-volume relation to be numerically the same, thus to identify $\varepsilon_0 = 4B$.

There is a further, much more important property which both models share: the exponential mass spectrum [10, 11]. Since the mass spectrum and the particle volumes determine together the thermodynamical behaviour of our system, the hadron gas seen as a SBM cluster system is identical to a hadron gas seen as a gas of bags up to and including the critical curve $T(\mu)$. Thus SBM is—as a thermodynamic model—fully equivalent to a gas of QCD bags [12]. Our clusters are excited QCD bags and choosing the pion and the nucleon as

input (instead of quarks) amounts to imposing local colour neutrality inside the bags and accepting Nature's own solution of the QCD bound-state problem (*).

Once this is accepted, it is clear what must be on the other side of the critical curve: since on the critical curve all clusters ≡ bags have coalesced into one infinite supercluster ≡ superbag, the matter on the other side of the critical curve is no longer a more or less dense gas of clusters: *it has there become the very matter which is inside bags: a quark-gluon plasma* [5, 12-14]. As such, it possesses the properties of a black-body radiation of an almost massless gas of only a few species (flavours × colours) with feeble interaction.

1˙3. *The infinitely extended hadron phase in* SBM. – Going back to the hadron phase, we list a few more quantitative properties near the critical curve. The model allows a simple straightforward calculation of densities, like baryon number density, number density of baryons + antibaryons, pions, kaons, ..., energy density, cluster number density and, important in our context, of the average mass and volume of clusters as well as of transverse-momentum distributions.

All numerical results in this paper are computed with a model having the following parameters [5]:

$$\text{(1.3)} \qquad \begin{cases} B^{\frac{1}{4}} = 0.145 \text{ GeV (bag constant)}, \\ T_0 := T_c(\mu = 0) = 0.19 \text{ GeV}, \\ \mu = 0. \end{cases}$$

Only $\mu = 0$ is here specially adapted to the situation ($p\bar{p}$), the other two paramenters have not been fitted to the present experiments; their values had been chosen (**) in 1980 (for application of the model to relativistic heavy-ion collisions [5]). In so far, the results displayed in this paper are predictions; the most characteristic being the following ones.

While *all* densities and $\langle p_T(T)\rangle$ go to finite values on the critical curve, the average cluster mass $M(T)$ and the average cluster volume $\langle V(T)\rangle$ go to ∞ there [8] (for details see subsect. **2**˙2):

$$\text{(1.4)} \qquad \begin{cases} \langle M(T)\rangle \Rightarrow \text{const} \cdot (T_0 - T)^{-1}, \\ \langle V(T)\rangle = \langle M(T)\rangle / 4B. \end{cases}$$

(*) In the very spirit of the SBM the input particles need not be really « elementary », they serve as building blocks of all *higher* composite states. For our purposes the pion and the nucleon do suffice, while ρ and Δ would not, because pions and nucleons do exist as *free* particles; quarks, however, do not (so far) exist free.

(**) T_0 is not really a free parameter; it is calculated from the BE which, however, contains another parameter m_0 lying between m_π and m_N [6, 9].

Figures 1.5*a*) and *b*) show some particle number densities (here in an irrelevant normalization: number per « nucleon volume »).

Figure 1.6*a*) displays the average cluster mass $\langle M(T)\rangle$ as a function of T and fig. 1.6*b*) the same as a function of $\langle p_T(T)\rangle$ (see subsect. **3**'2). It is seen that at $p\bar{p}$ collider energies cluster masses from 300 MeV to more than 10 GeV

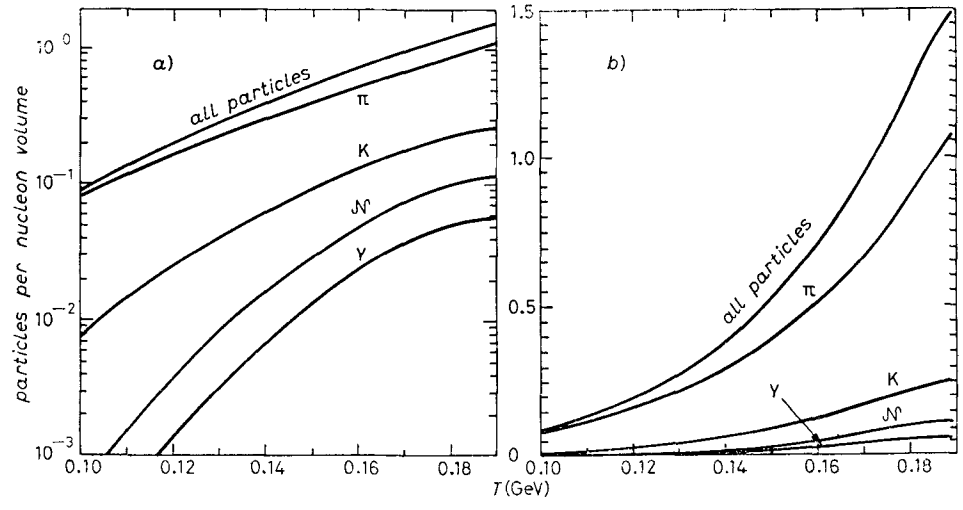

Fig. 1.5. – Particle number densities as following from the SBM [5]: *a*) logarithmic plot, *b*) linear plot as functions of the temperature ($\mu = 0$).

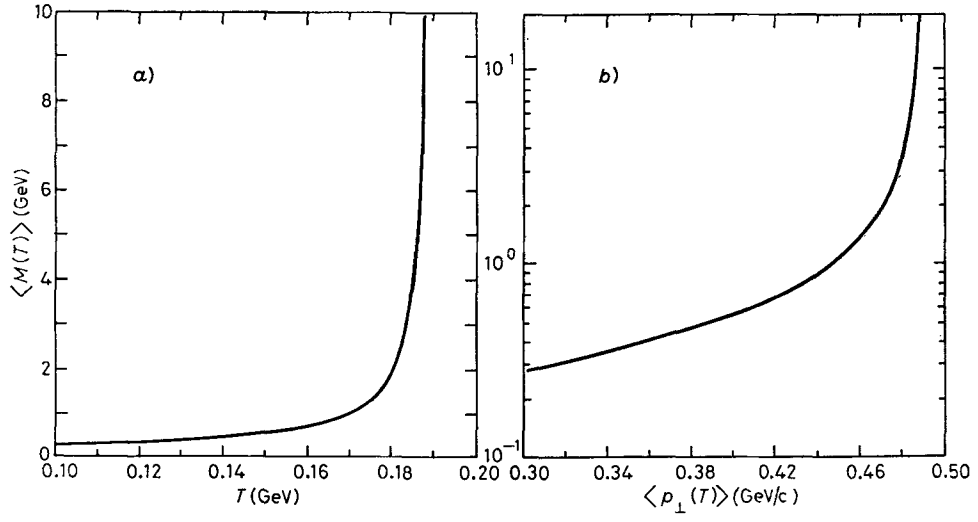

Fig. 1.6. – The average cluster mass as following from the SBM [5, 8] as a function of *a*) the temperature and *b*) the average transverse momentum as calculated in the same model ($\mu = 0$).

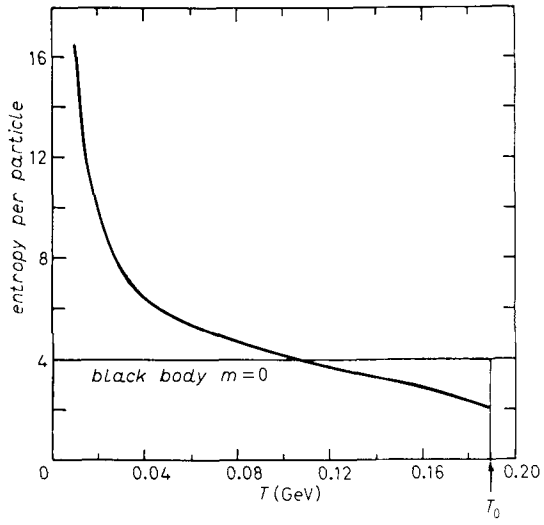

Fig. 1.7. – Entropy per particle as a function of the temperature as calculated in the SBM [5] ($\mu = 0$).

should currently occur ($0.3\ \mathrm{GeV/c} \leqslant \langle p_T \rangle \leqslant 0.48\ \mathrm{GeV/c}$), possibly leading to a bumpy structure of the rapidity distribution in event-by-event plots.

Figure 1.7 shows the entropy per particle as a function of the temperature. A commonly used rough estimate is that the entropy S is proportional to the number of particles produced. This is exactly true for a black-body radiation

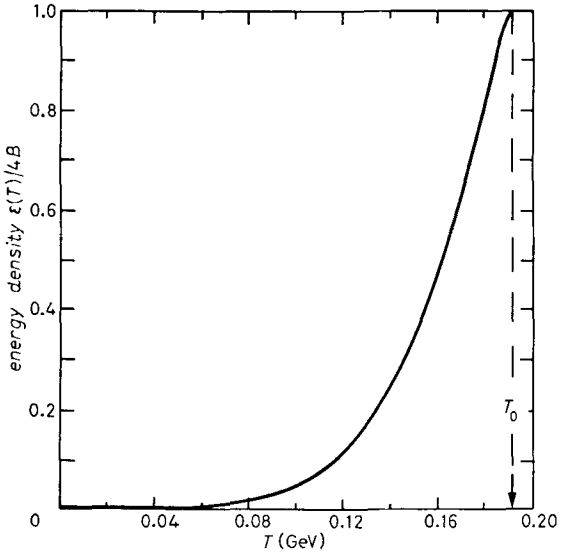

Fig. 1.8. – Energy density *vs.* temperature from the SBM [5] ($\mu = 0$) normalized to $\varepsilon_0 = 4B$. Note that ε remains rather small up to $T/T_0 \leqslant 0.6$ implying that most observed particles come from regions with T of order T_0.

of massless particles, where $S/N = 4$ independent of T and of the number of species of particles. In our case it is only approximately true at low particle numbers, but it becomes true (with $S/N \to 2.04$) for large particle numbers ($T \to T_0$), because for $T \to T_0$ the entropy density as well as the total particle number density go to finite constants.

In fig. 1.8 we display the energy density ε (normalized to $4B$, the bag energy density) *vs.* temperature ($\mu = 0$). Note the steep rise of ε between $0.12 \leqslant \leqslant T \leqslant T_0$; it has the consequence that one finds experimental temperatures hardly ever outside this interval (see below).

The most important property shown in this figure is that (due to finite particle volumes) ε reaches a *finite* limit as $T \to T_0$; therefore, the transition temperature can actually be *attained*—and not only approached asymptotically for $\varepsilon \to \infty$ as in earlier versions of the SBM (where, therefore, T_0 was claimed to be a limiting temperature).

1·4. *How the model is related to a real collision. – All this applies to infinitely extended hadronic matter in equilibrium.* Experiments unfortunately produce only microscopic lumps of such matter, which are never in equilibrium. The relation between the described model and the situation in a collision is, therefore, far from trivial. It seems, however, that at any given time equilibrium is nearly reached *locally*, so that the above model might be applied locally and then be folded with collective motions assumed *ad hoc* [15] or derived from special models [16].

Qualitatively a collision goes through the following stages: the two colliding particles will, in the overlap region, slow down and compress each other, whereby locally kinetic energy is changed into internal-energy density (heat). In energetic collisions the so-produced energy density ε will, in the overlap region, be larger than $4B$, so that the system (locally) enters more or less in the quark gluon phase and reaches there a temperature $T \sim \varepsilon^{\frac{1}{4}}$, which may be considerably higher than T_0. Then it expands and cools until it reaches the critical curve, where it breaks up into hadronic clusters. In less central regions or in peripheral collisions the energy density might remain below $4B$ and there the system does not enter into the quark gluon phase. The steep rise of $\varepsilon(T)$ shown in fig. 1.8 has, however, the consequence that even then the temperature will not be much below T_0, so that we may expect that over large parts of the rapidity distribution the apparent temperature in very-high-energy collisions is near T_0: in the very central region because the system returns from the quark gluon phase and breaks up into hadrons at T_0; in the other regions because it reaches $T \leqslant T_0$ even at moderate energy densities. Since, moreover, particle production disappears exponentially with falling temperatures (fig. 1.5*a*), *b*)) most produced particles come from regions with temperatures of order $0.14\ \mathrm{GeV} \leqslant \leqslant T \leqslant T_0$, which, as argued, might be reached up to nearly the ends of the rapidity distribution. Therefore, in the central region $\left(|y| \ll \ln\left(\sqrt{s}/m\right)\right)$ we

expect $\langle p_T \rangle$ corresponding to $\approx T_0$, while even near the ends $\left(|y| \leqslant \ln(\sqrt{s}/m) - 1\right)$ we still might have $\langle p_T \rangle$ corresponding to ≈ 0.14 GeV, only about 20 % less than at $y=0$ (see fig. 3.3*b*)). Thus in very-high-energy collisions $\langle p_T(y) \rangle \simeq$ const (within $\approx 20\,\%$) over most of the rapidity distribution. This is a qualitative but characteristic prediction of our model. It could not be made in statistical-thermodynamical models *not* possessing a critical temperature (phase transition).

The present observations hold, of course, only on the average. If one triggers for *special* events, one will find characteristic deviations, one of which we here are precisely interested in: namely $\langle p_T \rangle$ *vs.* central multiplicity (subsect. **3**˙3).

While most emitted particles originate from the decay of hadronic clusters at temperatures $T \leqslant T_0$, very few may escape already from the plasma phase. This can happen in two ways: either on the surface of the quark-gluon blob a q and a $\bar{\text{q}}$ are near to each other and, at the same time, have a relative momentum such that a meson could be formed (mostly π; baryons would need the conspiration of there quarks) which then might escape with a momentum typical for the local temperature of the plasma at that moment; or a single *very* energetic (at the tail of the momentum distribution) quark or gluon tries to escape alone and, since confinement forbids this, it has to hadronize by dragging a tail of $\text{q}\bar{\text{q}}$ pairs behind and giving rise to a jet of hadrons which will have an internal momentum distribution whose average (in jet direction) should again correspond roughly to the local plasma temperature. (Very energetic jets from single hard scattering would not fall under this category though an average over not so extremely energetic hard-scattering processes might.) These two mechanisms would give rise to the main part of the well-known large p_T (those whose distribution takes off at $p_T \approx 1.5$ to 2 GeV/c from the underlying Boltzmann-like distribution characterized by $T \approx T_0$; see fig. 1.3) which, in our interpretation, would thus probe the quark-gluon plasma directly [17-21].

What is the difference between the quark-gluon plasma at $T \gg T_0$ and the big clusters near T_0 which inside also consist of quarks and gluons? Why do the latter break up so easily, while the former allow only occasionally the escape of a hadron? From the point of view of the statistical-bootstrap model the large clusters near T_0 (while being filled with a quark-gluon plasma) are still composed of *hadrons*, which amounts to saying that colour neutrality is locally satisfied in subregions of nucleon size (much smaller than the whole cluster): such a cluster has no difficulty to rapidly disintegrate into the already preformed hadrons.

Above the critical curve this short-range colour correlation is no longer enforced; the mechanism which did so has broken down (because of the singularity in the partition function describing clusters in clusters in clusters). This makes the escape of hadrons more difficult.

If one does not intend to test a hybrid model in which collective and thermal motions are superimposed [15, 16, 22], then only transverse momenta and

multiplicities being invariant under collective motions (p_T only under longitudinal ones) remain as means of testing the above ideas by confronting experimental data with quantities calculated from equilibrium thermodynamics. This will be done in sect. **2** to **4**.

In appendix A we discuss possible distorting mechanisms, which presently will be ignored.

In appendix B we shall show why the « measured $\langle p_T \rangle$ » might not always be the true $\langle p_T \rangle$ and propose a safer method to determine them. Our notation will be that of ref. [5-8].

2. – Thermal and hadrochemical equilibrium.

We consider an infinitely extended hadron gas in equilibrium as described by the statistical-bootstrap model [5-8], called « SBM gas ».

2'1. *Transverse momentum* p_T. – If one neglects Bose and Fermi statistics, a particle of mass m has at temperature T a momentum distribution (for a complete derivation with statistics and longitudinal motions see [23])

$$f(\boldsymbol{p}, m, T)\,\mathrm{d}^3p = \mathrm{const}\cdot\exp\left[-\sqrt{\boldsymbol{p}^2 + m^2}/T\right]\mathrm{d}^3p\ ; \tag{2.1}$$

writing $\boldsymbol{p}^2 = p_T^2 + p_\parallel^2$ and integrating over $p_\parallel$, one obtains, with $\mathrm{d}^2p_T \equiv 2\pi p_T^2\,\mathrm{d}p_T$ and $p_T = |\boldsymbol{p}_T|$, the p_T distribution

$$\frac{\mathrm{d}N(p_\perp, m, T)}{\mathrm{d}p_\perp} = \mathrm{const}\, p_\perp \cdot \sqrt{p_\perp^2 + m^2}\, K_1\left(\sqrt{p_\perp^2 + m^2}/T\right) \tag{2.2}$$

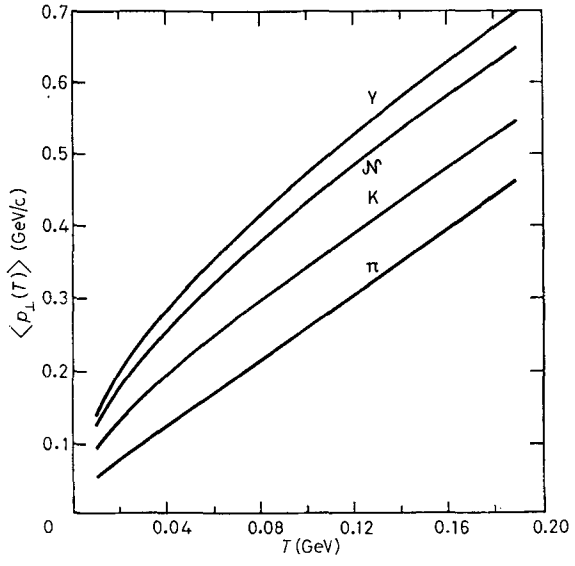

Fig. 2.1. – Average transverse momenta (Boltzmann approximation) as functions of the temperature according to eq. (2.3).

and the mean p_T

$$\langle p_\perp(m, T)\rangle := \frac{\int_0^\infty p_\perp (\mathrm{d}N/\mathrm{d}p_\perp)\,\mathrm{d}p_\perp}{\int_0^\infty (\mathrm{d}N/\mathrm{d}p_\perp)\,\mathrm{d}p_\perp} = \sqrt{\frac{\pi}{2} mT}\,\frac{K_{\frac{3}{2}}(m/T)}{K_2(m/T)}\,. \tag{2.3}$$

These formulae—which are model independent—have been first derived with Bose and Fermi statistics incorporated by IMAEDA [24]; see also appendix B.

Figure 2.1 shows $\langle p_T(M_1 T)\rangle$ for m_π, m_K, m_N and $m_Y = 1.175$ (mean value Λ and Σ). Dividing eq. (2.3) by either m or T leads to universal functions of m/T on the r.h.s:

$$\left\{\begin{array}{l} \langle p_\perp\rangle/T =: v\,, \qquad \langle p_\perp\rangle/m =: w\,, \qquad m/T =: z\,; \\ \hline v = \sqrt{\frac{\pi z}{2}}\,\frac{K_{\frac{3}{2}}(z)}{K_2(z)} \begin{cases} \sqrt{\frac{\pi z}{2}} & \text{for } z \to \infty\,, \\ \frac{3\pi}{4} & \text{for } z \to 0\,; \end{cases} \\ \hline w = \frac{v}{z} = \sqrt{\frac{\pi}{2z}}\,\frac{K_{\frac{3}{2}}(z)}{K_2(z)} \begin{cases} \sqrt{\frac{\pi}{2z}} & \text{for } z \to \infty\,, \\ \frac{3\pi}{4z} & \text{for } z \to 0\,. \end{cases} \end{array}\right. \tag{2.4}$$

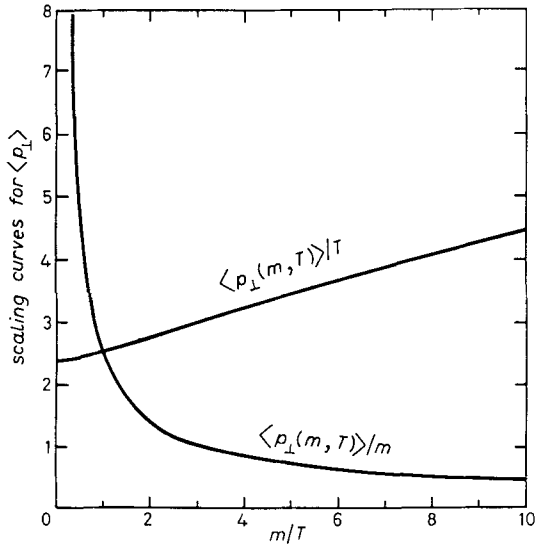

Fig. 2.2. – Universal scaling curves for the average transverse momentum: $\langle p_T\rangle/T$ and $\langle p_T\rangle/m$ as a function of m/T as following from eqs. (2.4).

The curves in fig. 2.2 display v and w as functions of z; whenever two of the three variables $\{\langle p_T \rangle, m, T\}$ are known, the third follows from fig. 2.2.

2·2. *Particle number densities, entropy density, pressure and average cluster mass.* – We describe the SBM hadron gas by a procedure [5-8] in which the *extended-particle* quantities can be simply expressed in terms of the *point-particle* partition function $Z_{pt}(\beta, V, \lambda \ldots)$, which is explicitly known [5, 25] and from which point-particle densities (energy, entropy, particle numbers, pressure ...) follow as usual:

energy density ε_{pt}:

$$\varepsilon_{pt}(\beta, \lambda, \ldots) = -\frac{1}{V}\frac{\partial \ln Z_{pt}}{\partial \beta}; \tag{2.5}$$

baryon number density ν_{pt}:

$$\nu_{pt}(\beta, \lambda_B, \ldots) = \frac{1}{V}\lambda_B \frac{\partial \ln Z_{pt}}{\partial \lambda_B}; \tag{2.6}$$

pion number density π_{pt}:

$$\pi_{pt}(\beta, \lambda_\pi, \ldots) = \frac{1}{V}\lambda_\pi \frac{\partial \ln Z_{pt}}{\partial \lambda_\pi} \tag{2.7}$$

and similarly for strange particles (K, Y). The corresponding quantities for *extended* particles are then found by the rule [5-8]

$$\textit{intensive quantity for extended particles} = \frac{\textit{intensive quantity for point particles}}{1 + \varepsilon_{pt}(\beta, \lambda, \ldots)/4B}. \tag{2.8}$$

From the definition as derivatives with respect to a fugacity it follows that particle number densities refer to final particles after decay of all clusters.

The entropy density $\sigma = S/V$ is

$$\sigma = \frac{\sigma_{pt}}{1 + \varepsilon_{pt}/4B} = \frac{(1/V)\ln Z_{pt} + (\varepsilon_{pt} - \mu\nu_{pt})/T}{1 + \varepsilon_{pt}/4B}, \tag{2.9}$$

where $\mu = T \ln \lambda$ is the baryon chemical potential. The pressure is

$$P = \frac{P_{pt}}{1 + \varepsilon_{pt}/4B} \tag{2.10}$$

with

$$P_{pt} = -\frac{T}{V}\ln Z_{pt}(\beta, V, \lambda). \tag{2.11}$$

It is remarkable that the pressure obeys an « ideal-gas equation » [8] in the form

$$P = \frac{\langle N_c \rangle}{\langle V \rangle} T , \tag{2.12}$$

where $\langle V \rangle$ is the expectation value of the total volume (which is not fixed) of the system and $\langle N_c \rangle$ the expectation value of the *number of clusters* present; while each of these two is ∞, their ratio is a finite, well-behaved function of μ and T. That we obtain the ideal-gas equation in these variables is not in contradiction with our claim to describe a strongly interacting system: while in the case of a truly ideal gas N and V are fixed external parameters, they are here dynamical variables (functions of μ and T). It turns out that near the critical curve $\langle N_c/V \rangle \to 0$ and $P \to 0$. There, however, the system is instable ($dP/dV > 0$), so that a Maxwell construction is necessary from which a first-order phase transition results with P everywhere finite > 0.

Finally, the average cluster mass [8]: as the temperature is limited to T_0 (of order m_π), most clusters (except the π itself) are moving with nonrelativistic velocities, so that the total energy carried by a cluster of mass M is in good approximation

$$E_{\text{cluster}} \approx M + \tfrac{3}{2} T , \tag{2.13}$$

hence, by averaging, the total energy

$$\langle E \rangle \approx \langle N_c \rangle [\langle M \rangle + \tfrac{3}{2} T] \tag{2.14}$$

and, with eq. (2.12),

$$\langle M \rangle \approx \frac{\langle E \rangle}{\langle V \rangle} \frac{\langle V \rangle}{\langle N_c \rangle} - \frac{3}{2} T = \frac{\varepsilon_{\text{pt}}}{P_{\text{pt}}} - \frac{3}{2} , \tag{2.15}$$

which was shown in fig. 1.6*a*) and *b*) as a function of T and $\langle p_T \rangle$. For $T \to T_0$, these formulae become exact.

These and other quantities are available through simple and short computer programs based on the model described in ref. [5-9]. All curves shown here were calculated with these programs and the parameters (1.3).

3. – Approaching the phase transition.

When the critical curve is approached, all above point-particle densities diverge; the extended-particle ones reach finite limits (since they are divided by the diverging ε_{pt}); the energy density tends to $4B$, the entropy density ($\mu = 0$) to $4B/T_0$, etc.

As all variables are functions of the temperature, one can plot any one against any other using the temperature as a parameter. We present here a few of the many possible combinations.

3·1. *Charged-particle number ratios.* – We define the ratios

$$R_i(T) := \{\langle N_i(T)\rangle / \langle N_\pi(T)\rangle\}_{\text{charged}} \tag{3.1}$$

and show in fig. 3.1 these ratios for kaons, nucleons and hyperons as functions of the total charged multiplicity emerging from an average cluster. While the ratios tend to finite limits at the transition temperature, the average multiplicity per cluster diverges with the cluster mass; hence the ratios level off for $\langle N\rangle_{ch} \to \infty$.

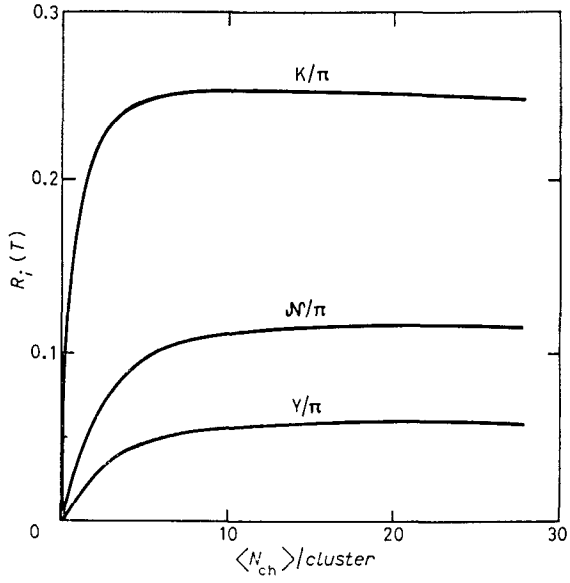

Fig. 3.1. – The ratios K/π, N/π, Y/π (charged) as functions of the mean charged multiplicity emitted by an average cluster as calculated from the SBM [5].

If one would measure R_i as functions of dN_{ch}/dy, curves of this shape should result. The same ratios are plotted in fig. 3.2 as a function of $\langle p_T(T)\rangle$. The bending down at the end (when $T \to T_0$) is due to the still steeply rising π production (see fig. 1.5). As the total $\langle p_T(T)\rangle$ is an almost linearly rising function of the temperature, (see fig. 3.3) a plot of the ratios *vs.* T would look very similar.

A comparison of these predictions with experimental data is difficult for reasons discussed in the introduction (model: infinite matter in equilibrium; experiment: microscopic collective motions with only approximate local equi-

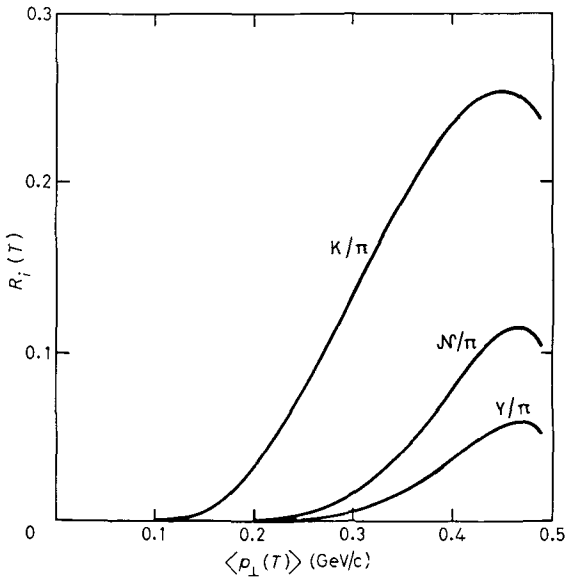

Fig. 3.2. – Charged-particle ratios (as in fig. 3.1) as functions of the average transverse momentum $\langle p_T(T)\rangle_{\text{all particles}}$ as calculated from the SBM [5].

librium) and also since charged multiplicites have been measured (more precisely, estimated) only as averages over the rapidity interval $-5 \leqslant y \leqslant 5$ accessible to the UA 5 detector [26]. Therefore, between the model and the experiment various further averaging processes enter which depend partly on the physics (*e.g.*, collective motions) and partly on the experimental set-up (*e.g.*, acceptances).

We shall nevertheless confront our results with the experiment. Our table shows in the first column the ratios as taken from table II of ref. [26]; the second gives our ratios in the interval $0.3\ \text{GeV/c} \leqslant p_T(T) \leqslant p_{T\,\max}(T_0)$, the third the factor by which they vary in this p_T interval and the fourth our values at the measured $\langle p_T\rangle_{UA1}$ [4].

TABLE I. – *The ratios* $R_K = N_K/N_\pi$, $R_B = N_{\text{baryon}}/N_\pi$, $R_Y = N_{\text{hyperon}}/N_\pi$.

Ratio	UA5	Model fig. 3.2	Factor of variation	Model fig. 3.2 at $\langle p_T\rangle_{UA1}$
R_K	0.11	0.14 ÷0.25	2	0.24
R_B	0.07	0.02 ÷0.11	5	0.09
R_Y	0.01	0.005÷0.055	10	0.04

The estimated UA5 values [26] lie near to or within the interval chosen in fig. 3.2. There is, however, no $\langle p_T(T)\rangle$ at which we could reproduce all experimental values simultaneously (which is indeed not to be expected). At $\langle p_T\rangle_{UA1}$ we over-estimate R_K by a factor 2, R_Y by 4, while R_B is about correct.

Is this a satisfactory agreement or a catastrophic disagreement? We believe neither, for the following reasons which again derive from the wide trench between the idealizing model and the reality of a collision:

i) We use [5] the grand canonical formalism, which is justified in the thermodynamical limit (infinite system; $t \to \infty$), while in the experiment we have an extremely small space-time region. With decreasing volumes grand canonical results become gradually less and less reliable. As a simple example consider pair production ($p\bar{p}$, $K\bar{K}$, ...). In the grand canonical formalism one uses chemical potentials (here $\mu = 0$) and finds an equilibrium population of pairs (leading factors, order of magnitude)

$$N_{pair} \sim \exp\left[-\frac{m}{T}\right], \qquad \text{large volume}. \tag{3.2}$$

If the volume is not infinite, the equilibrium population depends on the volume, such that for very small volumes one obtains [23]

$$N_{pair} \sim \exp\left[-\frac{2m}{T}\right], \qquad \text{small volume}. \tag{3.3}$$

As discussed in detail in ref. [27], the volume in a pp collision is « small » and the equilibrium population calculated in the grand canonical formalism may be too large by a factor of ≈ 2. Reducing our values by a factor of 2 would make the overall agreement better.

ii) The previous remark still applies to equilibrium. If the time is short, « chemical » equilibrium may be only more or less approached. Here again the population at time t will be smaller than at $t \to \infty$ [28].

iii) Our fig. 3.2 shows

$$R_i(T) = \frac{\langle N_i(T)\rangle}{\langle N_\pi(T)\rangle} =: F_i(\langle p_\perp(T)\rangle) \tag{3.4}$$

and this is, within the model, a unique functional relation between R_i and $\langle p_T(T)\rangle$. Assume this relation to be indeed *locally* true in a collision; then the variation of T over the whole space-time region as well as the influence of experimental cuts etc. may be characterized by an unknown *temperature distribution* $W(T)$, normalized to unity.

We then shall have to integrate our local functions with weight $W(T)$ over T; so that, in general,

$$\langle N_i\rangle_{expt} \neq \langle N_i(\langle T_{expt}\rangle)\rangle \tag{3.5}$$

and

$$\langle R_i \rangle_{\text{expt}} \neq F_i(\langle p_\perp \rangle_{\text{exot}}) \,. \tag{3.6}$$

One should not even expect to find a single $\langle p_T \rangle$ at which the $\langle R_i \rangle_{\text{expt}} = R_i$ for all i.

iv) In view of these remarks, of the strong variation of the R_i (column 3 of the table) and of the experimental uncertainties we may claim that our model is not in difficulty with respect to charged-particle ratios.

3·2. *The mean transverse momentum.* – Let $n(m, T)$ be the mean *charged*-particle number density of the species with mass m. As the mean transverse momentum is a function of the mass and of the temperature, the total mean transverse momentum of charged particles is

$$\langle p_\perp(T) \rangle = \frac{\sum_m n(m, T) \langle p_\perp(m, T) \rangle}{\sum_m n(m, T)} \,. \tag{3.7}$$

This function, with m running from pions to hyperons, is shown in fig. 3.3*a*) together with the individual *weighted* contributions of pions, nucleons, kaons and hyperons to the total. Note that the weighted contributions of eq. (3.7) must not be confounded with the $\langle p_T \rangle$ these particles do actually have and

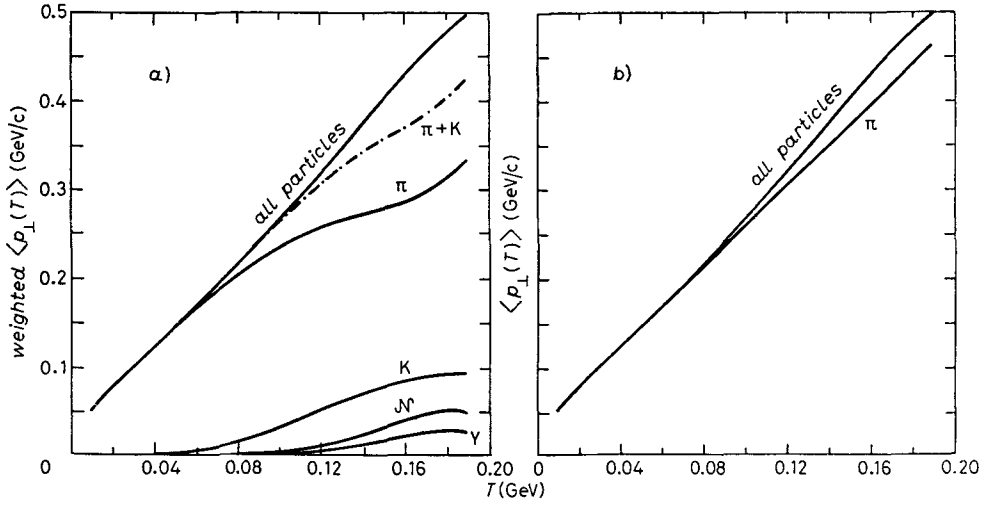

Fig. 3.3. – *a*) Total $\langle p_T(T) \rangle$ as function of the temperature together with its individual (weighted) components (π, K, N, Y) according to eq. (3.7) evaluated in the SBM [5] ($\mu = 0$). *b*) Total $\langle p_T(T) \rangle$ and $\langle p_T \rangle_\pi$ as functions of the temperature (eq. (3.7) and SBM [5], eq. (2.3)) ($\mu = 0$).

which are shown in fig. 2.1. In fig. 3.3*b*) we show the total $\langle p_T(T)\rangle$ together with the actual transverse momentum of pions. This figure illustrates a source of error in determining a « temperature » from $\langle p_T\rangle$: take $\langle p_T\rangle = 0.45$; if one takes into account all particles one concludes $T = 0.168$ GeV, but if one had erroneously assumed that the contribution of heavier particles was negligible due to their rarity, one would have taken the pion curve and found $T = 0.184$ GeV.

As the curves in fig. 3.3*a*) and *b*) have been computed at $\mu_{\text{baryon}} = \mu_{\text{strange}} = 0$, heavier particles contribute only via pair and associated production. These figures are, therefore, specific to $p\bar{p}$ collisions; in pp and even more in heavy-ion collisions ($\mu \neq 0$) baryons would increasingly contribute and $\langle p_T\rangle_{\text{total}}$ would rise higher above the pion curve.

3˙3. *The dependence of p_T on the multiplicity.* – The experimental relation between $\langle p_T\rangle$ and the mean charged multiplicity per unit rapidity interval was depicted in fig. 1.1.

Such a relation could be calculated quantitatively in a hybrid model containing thermodynamics coupled with collective motions [15, 22]. As we here wish mainly to see whether the *existence of a phase transition* shows up in this relation, we try a simple semi-quantitative connection between model and experiment. Let

$$n(T) := \sum_m n(m, T) \tag{3.8}$$

be the total charged-particle number density. In a given volume V the total number is then $N = nV$—but what is the volume V corresponding to the rapidity interval $\Delta y = 1$?

A first guess is that it might be proportional to the average cluster volume $\langle V_c(T)\rangle = \langle M(T)\rangle/4B$:

$$\frac{\mathrm{d}N_{\text{ch}}^{(1)}}{\mathrm{d}y} = C^{(1)}(T)n(T)\langle M(T)\rangle/4B\,, \tag{3.9}$$

where $C^{(1)}(T)$ is the average number of clusters per unit rapidity.

A better guess starts from the observation that $n = N/V$ refers to a volume containing clusters plus empty space. To obtain $N = nV$ we, therefore, should take a volume made up of the average cluster volume V_c plus its average share of empty space. This is not difficult, since the energy density is defined in much the same way as the particle number density: $\varepsilon(T) = (M = 4B \cdot V_c)/(V = V_c + \text{empty space})$, so that

$$\frac{\langle V = V_c + \text{empty space}\rangle}{\langle V_c\rangle} = \frac{4B}{\varepsilon(T)}\,. \tag{3.10}$$

With this factor—which tends to 1 when the phase transition is approached—we should multiply the r.h.s. of eq. (3.9) in order to replace the cluster volume V_c by the correct reference volume

$$\frac{\mathrm{d}N_{\mathrm{ch}}^{(2)}}{\mathrm{d}y} = C^{(2)}(T)n(T)\langle M(T)\rangle/\varepsilon(T)\,. \tag{3.11}$$

Finally, we argue that in front of the other rapidly varying factors—$M(T)$ diverges for $T \to T_0$—we may treat the two unknown functions $C^{(1,2)}$ as constants. All other factors are calculable in the model.

The three full curves of fig. 3.4 represent eq. (3.9) with $C^{(1)} = \{6, 9, 12\}$, the broken curve eq. (3.11) with $C^{(2)} = 3.5$. None gives a perfect fit (which should not even be attempted—see appendix B), but all show the correct trend, which is extrapolated in fig. 3.5 (eq. (3.9), $C^{(1)} = 9$). Remember that $C^{(1)}$ and/or $C^{(2)}$ are here the only free parameters.

3·4. *Interpretation.* – The present model does not try to explain how in the central region a variation of the temperature can arise; it only asserts that, if it is there, corresponding variations of $\langle p_{\mathrm{T}}(T)\rangle$ and $\mathrm{d}N_{\mathrm{ch}}/\mathrm{d}y$ must occur. When $T \to T_0$, then $\langle p_{\mathrm{T}}\rangle$ goes to a finite limit, while $\mathrm{d}N_{\mathrm{ch}}/\mathrm{d}y$ diverges; therefore, the general shape of the curves is independent of detailed assumptions.

In more elaborate models with longitudinal collective motions [15] a variation of the temperature is linked to the degree of thermalization reached locally; at

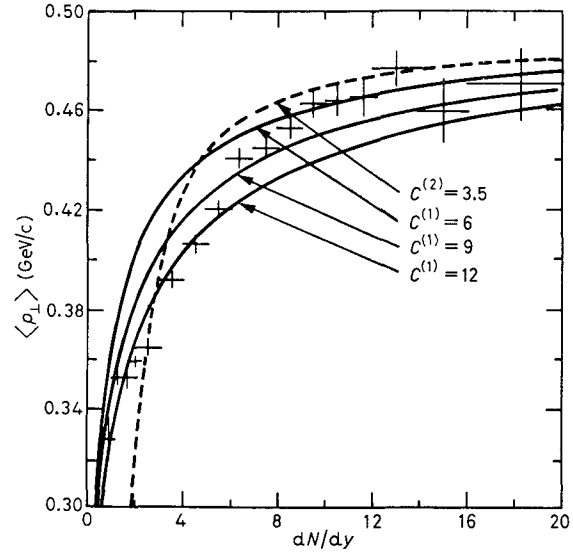

Fig. 3.4. – Mean transverse momentum $\langle p_{\mathrm{T}}\rangle$ as a function of the charged multiplicity per unit rapidity. The four different curves are calcultaed from eq. (3.9) (upper full curve $C^{(1)} = 6$, middle $C^{(1)} = 9$, lower $C^{(1)} = 12$) and eq. (3.10) (broken curve $C^{(2)} = 3.5$). The crosses represent experimental data [4].

large impact parameters most of the incoming energy remains kinetic and the temperature remains low, while small impact parameters lead to better thermalization and higher temperatures as well as larger multiplicities. Sorting events with respect to multiplicities amounts *grosso modo* to sorting them with respect to impact parameter and/or to temperature.

The shape of the curves in fig. 3.4 and 3.5 is closely linked to the phase transition which the model predicts. Indeed, without the phase transition the average cluster mass and volume would not diverge at a finite transition temperature and $\langle p_T \rangle$ as a function of dN_{ch}/dy would not level off. The observed levelling has nothing to do with the kinematical limit which is still far away at $dN_{ch}/dy \approx 20$.

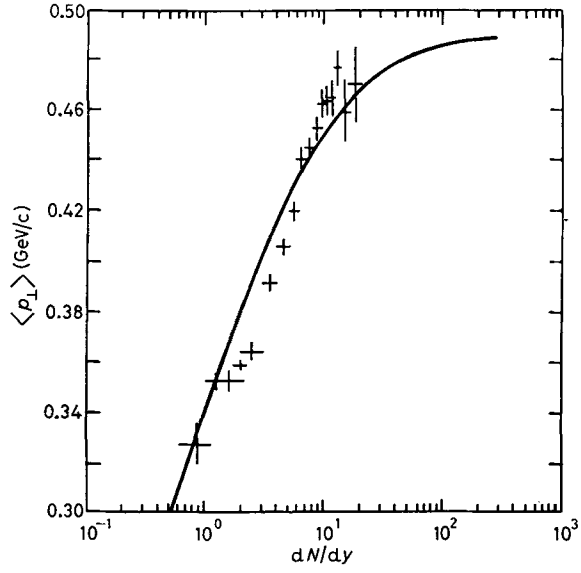

Fig. 3.5. – Extrapolation of $\langle p_T \rangle$ to large multiplicities (eq. (3.9) with $C^{(1)} = 9$.) Crosses as in fig. 3.4.

The present interpretation is only superficially different from that recently proposed by VAN HOVE [29] insofar as we do not explicitly invoke a *first*-order phase transition; however, the present model indeed strongly suggests that the transition is of first order, because near to the critical curve there is a region of instability requiring a Maxwell construction [7, 8]; in the present paper, this fact is disregarded, because it would rather strengthen than invalidate our conclusions.

Our approach to the problem is, however, different from the one chosen by BARSHAY [30], which also reasonably reproduces the data, but does not predict $\langle p_T(dN/dy) \rangle$ to level off. Measurements extended to $dN/dy \approx 30$ would already decide between the two models.

3·5. *Comparison* ISR/UA1. – In the introduction we have read off from fig. 1.1 three intriguing facts:

i) at small multiplicities the $\langle p_T \rangle$ of UA1 drop below those of ISR;

ii) the strong variation of $\langle p_T \rangle$ with dN/dY seen in UA1, which we just have claimed to have explained, is almost absent in the ISR data;

iii) flattening of the $\langle p_T \rangle$ curves occurs at ISR at significantly lower $\langle p_T \rangle$ than at UA1.

As decided in the introduction, we shall not worry about the first two points. Physical arguments make them unlikely to be true; moreover, the analysis given in appendix B shows that systematic errors might possibly explain them altogether.

Whatever the possible systematic errors may be, it seems that for larger multiplicities the ISR $\langle p_T \rangle$ do flatten at a lower value than the UA1 $\langle p_T \rangle$. This poses a problem for our model: if flattening is due to a phase transition —which would occur at a *fixed* temperature (*)—,then the corresponding $\langle p_T \rangle$ should be the same.

Might there be two consecutive phase transitions [32], the first at the temperature corresponding to $\langle p_T \rangle_{ISR}$, the second at higher temperature corresponding to $\langle p_T \rangle_{UA1}$? Probably not, because, if at UA1 the second has been reached, the first must have been already passed over: one should see two flat regions, the lower coinciding with that of ISR; nothing of that sort is indicated by the data.

Could it be that at ISR mainly pions are produced and at UA1 many heavier particles (see fig. 2.1: heavier particles have, at the same T, larger $\langle p_T \rangle$), so that $\langle p_T \rangle_{UA1} > \langle p_T \rangle_{ISR}$? No, because if the $\langle p_T \rangle$ of the flat part do belong to a fixed critical temperature, then the ratios of particle numbers for different masses are determined by that same temperature, so that the $\langle p_T \rangle$ should be the same again.

We, therefore, should look for mechanisms which would make it possible to push up $\langle p_T \rangle$ with the collision energy without changing the critical temperature T_0. There are several possibilities.

a) *High cluster spin.* The qualitative explanation is simple: the two incoming particles have an orbital angular momentum $L_0 = p_0 b$ (b = impact parameter). In an intermediate stage a number of clusters plus leading particles appear which move with much less momentum and, therefore, smaller orbital momenta L_i which, in general, do not add up to L_0. The difference $L_0 - \sum L_i = \sum S_i$ must then reappear in cluster spins. In any statistical-thermodynamical

(*) The differences between pp and $p\bar{p}$ collisions are irrelevant [31], since also for pp the chemical potential $\mu \approx 0$ in the central y region.

model with clusters, the latter do have spin; however, *only as a statistical fluctuation* with $\langle S \rangle = 0$ and $\sqrt{\langle S^2 \rangle} \approx \sqrt{M/2m_\pi}$; for such a gas of clusters our $\langle p_T(T) \rangle$ holds. If, however, something forces the clusters to have systematically $\langle S \rangle \neq 0$, then one would expect another $\langle p_T \rangle$. Indeed, it has been known for a long time [33] that the decay multiplicity $n(M, S)$ decreases with growing S for fixed M; consequently the mean kinetic energy and thus $\langle p_T \rangle$ must grow. A detailed analysis [34] shows that

under favourable production conditions the spins of clusters can grow proportional to their mass;

momenta in the plane orthogonal to the spin axis are strongly enhanced, while those parallel to the spin remain practically unchanged (intuitively obvious: centrifugal forces);

in the spin-orthogonal plane the angular distribution in *an event-by-event* analysis is—contrary to intuitive expectation—anisotropic and simulates a two-jet structure.

The average initial orbital angular momentum L_0 is about 150 at ISR and 1500 at UA1; it seems conceivable that with a 10 times larger L_0 there will be also more clusters with higher spins; this would automatically lead to larger $\langle p_T \rangle$ at UA1 than at ISR—although the temperature should be the same (it might then be not ≈ 0.190 GeV, but rather ≈ 0.160 GeV; this latter value was considered the most likely one some years ago, theoretically [35-37] and experimentally [38, 39]).

b) *Collective transverse motion.* The existence of such motions as well as of shock waves has been made likely by hydrodynamical calculations [40-43] in the case of heavy-ion collisions; it is not daring to conjecture their presence also in pp and $p\bar{p}$ collisions, in particular if the system enters into the quark-gluon phase and there expands. It is conceivable that such transverse motions might become more violent with increasing collision energy and make $\langle p_T \rangle$ larger at UA1 than at ISR. Some remarks about the kinematics are found in ref. [44].

c) *Influence of the high-p_T tail.* In appendix A we make a rough estimate of how the large-p_T tail of the p_T distribution could influence $\langle p_T \rangle$. The estimate assumes that the p_T distribution can be approximated by a superposition of decreasing exponentials, the first being fixed with a temperature $\approx T_0$ giving the low-energy $\langle p_T \rangle$, while the tail exponential has a « temperature » depending on the collision energy. Assuming for the sake of illustration only two superimposed exponentials (*), we find that at ISR the tail pushes $\langle p_T \rangle$ by about $(2 \div 3)\%$, while at UA1 it pushes $\langle p_T \rangle$ by about 15% (fig. A.4); this could almost explain the difference.

(*) One needs three or more.

Certainly all these mechanisms contribute to the difference in $\langle p_T \rangle$ for ISR and UA1 and it will be very difficult to disentangle them. The point is, however, that they produce different $\langle p_T \rangle$ without needing different temperatures. Therefore, there seems to be no inconsistency.

4. – Beyond the phase transition.

Beyond the phase transition we enter into the quark-gluon plasma. In the introduction we have claimed that the very large p_T can be interpreted as being due to particles escaping from the plasma before it cools down to transition temperature and total hadronization.

Such a picture is complementary, but not necessarily contradictory to QCD hard scattering; in fact, it could possibly result from an average over many hard-scattering processes. If it were true, it should be possible to calculate the large-p_T distribution from the properties of the quark-gluon plasma. We do that now.

4·1. *Energy density of a quark-gluon plasma.* – In order to keep things simple, we assume quarks and gluons to be noninteracting and massless. For such a (black body) gas the Stefan-Boltzmann law reads (σ_{St} is the usual Stefan constant; $\pi^2/15$ for QED):

$$\varepsilon = \sigma_{St} T^4 , \qquad \sigma_{St} = \frac{\pi^2}{30}\left(g_B + \frac{7}{8} g_F\right), \tag{4.1}$$

where $g_{B,F}$ = number of internal degrees of freedom of bosons and fermions, respectively. We put $g_B = 8$ (colour)·2 (helicity) = 16 (gluons), $g_F = 3$ (colour)· ·2 (helicity)·3 (flavour)·2 (antiparticle) = 36 (quarks), where we took into account u, d and s quarks only. Thus

$$\sigma_{St} = \frac{47.5}{30}\pi^2 = 15.6 , \qquad T = \left(\frac{E}{\sigma_{St} V}\right)^{\frac{1}{4}} . \tag{4.2}$$

4·2. *Energy density in a collision.* – For an order-of-magnitude estimate it suffices to assume that, in the overlap region of the colliding particles, matter has essentially come to rest and most of the energy is thermalized. If ΔV is the overlap volume and ΔE the energy contained therein, then from geometry $\Delta V/V_0 \simeq \Delta E/E$, where V_0 is about a nucleon volume and E the c.m. energy. Hence, independently of the impact parameter,

$$\varepsilon_{max} \approx E/V_0 \tag{4.3}$$

is the order of magnitude of the maximal possible energy density in the overlap region (we do not consider Lorentz-contracted volumes, since we assume matter in ΔV to have come to rest).

4·3. *The maximal collision temperature.* – With (4.3) and (4.2) we obtain

$$T_{\max} \approx E^{\frac{1}{4}} \left(\frac{1}{\sigma_{St} V_0}\right)^{\frac{1}{4}} \tag{4.4}$$

as the maximal collision temperature, if in the overlap region a plasma is formed. This is the upper limit of the temperature at the instant of collision at the hottest points; subsequently the plasma expands and cools down until the phase transition is reached. Particles escaping from the plasma should show a p_T distribution corresponding to a superposition of approximately termal distributions with temperatures ranging from $T_{\max}$ down to T_0. Therefore, the largest p_T might indeed measure $T_{\max}$.

4·4. *The tails of the p_T distribution.* – In fig. 4.1 we show p_T distributions as measured at ISR [45] and UA1 [4]. In order to eliminate the rising total

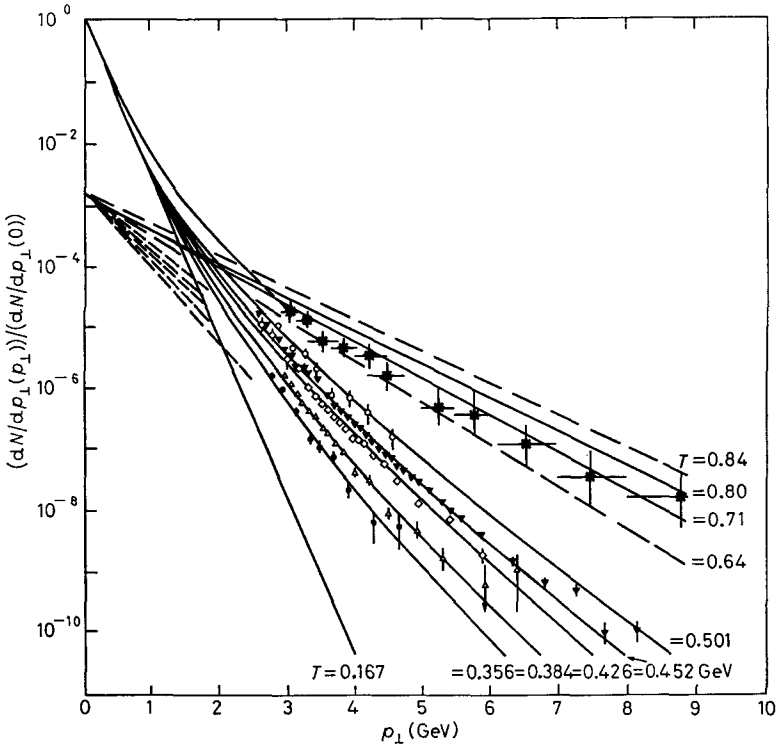

Fig. 4.1. – Inclusive p_T distributions with 23 GeV $< \sqrt{s} <$ 540 GeV. ISR [45] (π^0 only): • 23.5, ▵ 30.6, ◇ 44.8, ▾ 52.7, ○ 62.4; UA1 [4] (all charged): * 540. The high-p_T tails are fitted by hand; for UA1 four lines are drawn to see how the temperature T belonging to the slope varies within the experimental errors. It is possible without forcing to draw the lines such that they meet in one point at $p_T = 0$ lying by a factor $\approx$ 600 below that where all curves converge (= 1 by definition).

cross-section, we have normalized the curves to 1 at $p_T = 0$. This has the remarkable consequence that one can, within experimental errors, consider the high-p_T tails as straight lines meeting in one single point at $p_T = 0$. If we assume that these tails belong to particles escaping near T_{max}, this temperature can be read off from the slopes. To see what the uncertainties are, we have made a best eye fit to the ISR data and laid four straight lines through the UA1 data (shown in fig. 4.1). The ISR and UA1 data give in a $\ln T$ *vs.* $\ln E$ plot a set of points with rather large errors, but compatible with a linear interpolation (the errors are too large to allow more than that). Thus the data are compatible with the law [46]

$$T_{max} \approx aE^b \,. \tag{4.5}$$

The triples belonging to the four hand fits are

$$\begin{Bmatrix} a \\ b \\ T_{UA1} \end{Bmatrix} = \begin{Bmatrix} 0.164 \\ 0.26 \\ 0.842 \end{Bmatrix}; \quad \begin{Bmatrix} 0.165 \\ 0.25 \\ 0.795 \end{Bmatrix}, \quad \begin{Bmatrix} 0.168 \\ 0.23 \\ 0.714 \end{Bmatrix}, \quad \begin{Bmatrix} 0.171 \\ 0.21 \\ 0.641 \end{Bmatrix}. \tag{4.5a}$$

These numbers reflect the uncertainties of the fits and, therefore, of our interpretation.

4·5. *Comparison with the quark-gluon plasma.* – What should a and b be for a quark gluon plasma? Equation (4.4) gives the answer: if quarks were really massless ($m_q \ll T$), then $b = \frac{1}{4}$. The values of b obtained from the data lie indeed around that value.

With the preliminary assumption that V_0 is the ordinary nucleon volume $(4\pi/3)f^3 = 545\ (\mathrm{GeV})^{-3}$, we obtain from eqs. (4.2) and (4.4)

$$a_{QG} = \left(\frac{1}{\sigma_{St} V_0}\right)^{\frac{1}{4}} = 0.104\ [(\mathrm{GeV})^{\frac{3}{4}}] \tag{4.6}$$

also not much different from the experimental values.

We thus can state the remarkable fact that both, a and b, as calculated from a massless quark-gluon plasma, are near to the corresponding values deduced from the *assumption* that the physics behind the data is that of a quark-gluon plasma.

That the relevant volume should be an ordinary nucleon volume is not very likely: the violent shock of the collision will presumably do more than concentrate the available energy ΔE in an unperturbed volume $\Delta V = \Delta E \cdot V_0/E$; we rather expect that in addition the volume will be compressed to some smaller value (in the Fermi and Landau models the assumed volume compression even equals the Lorentz contraction before the collision). We can estimate by what

amount the volume should have been compressed, if our interpretation of the data were correct; for the effective interaction volume $\Delta V = \Delta E \cdot V_{int}/E$ we obtain from (4.5*a*) and (4.4)

$$\frac{V_0}{V_{int}} = \left(\frac{a_{expt}}{a_{QG}(V_0)}\right)^4 = 6.2 \text{ to } 7.3 . \tag{4.7}$$

Thus the compression factor is of order 6 to 7. This is considerably less than the still often assumed Lorentz contraction, which would require a compression factor $\gamma = 270$ (at UA1); the energy density would be 270 times, the temperature $(270)^{\frac{1}{4}} = 4$ times larger: 3.2 GeV, in plain contradiction with the slopes of the large-p_T tails. Moreover, T should be proportional to $\sqrt{E}$ instead to $E^{\frac{1}{4}}$ and this contradicts the data from ISR to UA1. One can conclude that the data —if our interpretation is correct—rule definitely out the old cherished «Lorentz-contracted interaction volume».

Whether our interpretation is correct or simply due to an accident is difficult to say. What speaks in favour of it is the logical consistency of the whole picture: theory suggests the existence of a phase transition with a transition temperature corresponding to the observed flattening of $\langle p_T \rangle$ and a quark-gluon plasma beyond with a temperature *vs.* energy relation corresponding to the observed high-p_T tails.

An analysis of experimental data leading to a clear distinction between «pure» QCD hard-scattering processes and a statistical-thermodynamical background or to the result that the *average* over the pure QCD processes behaves like coming from a plasma or simply disappears under the statistical-thermodynamical background in *inclusive* measurements—such an analysis is not yet possible.

Probably statistical thermodynamics of the plasma and perturbative QCD are complementary and compatible in a large overlap region, outside of which each of them has its proper domain of validity (where the other fails): QCD perturbative hard scattering for very-high-energy jets and the plasma description (with perturbative corrections [1, 2]) near to the transition region.

4·6. *Further remarks.* – The experimental data are compatible with the interpretation that the high p_T come from a quark-gluon plasma phase and measure directly the highest temperature it has reached during the history of a collision. It then would follow that this new phase had been entered already at ISR energies.

The fact that the straight lines in fig. 4.1 can, without forcing them, be drawn to meet in one single point is in itself interesting: it leads one to speculate that the ratio of the number of «leakage-from-the-plasma» events to that of ordinary ones (hadronizing at T_0) is approximately energy independent and of the order of 1:600 (see fig. 4.1).

At low p_T the UA1 distribution does not join the common straight line of all ISR distributions. This has several reasons: the ISR data in fig. 4.1 refer to π^0 only, while UA1 registers all charged particles. Therefore, UA1 should see systematically larger p_T (and a somewhat larger slope) (see fig. 3.3*b*)) than does ISR. Other reasons were discussed in subsect. **3**·5; all of them conspire to make $p_T(\text{UA1}) > p_T(\text{ISR})$ at all p_T.

Our present interpretation does not claim originality; proposals to see in large p_T a signature of superheating at a phase transition [15] or of a new phase of hadron matter actually having been reached have been made by many authors [17-21].

5. – Conclusion.

Do we see the phase transition hadron → quark-gluon plasma (predicted by so many models) at $p\bar{p}$ collider energies?

Yes; we even see it alrealy at ISR energies.

This conclusion might only be escaped if all speculations and calculations about this phase transition and the use of statistical thermodynamics in this context are senseless and if the consistency (though not detailed agreement) of their predictions with the experiment is due to some most unlikely accident.

The various distorting mechanisms entering between idealized thermodynamics and real collisions may affect numerical values; they cannot invalidate our conclusion.

* * *

Discussions with M. FAESSLER and J. RAFELSKI were very helpful; the latter drew my attention to the uncertainties in determining the experimental $\langle p_T \rangle$.

APPENDIX A

Distorting mechanisms.

We have, in the course of this paper, mentioned several times the wide gap between the idealized model of infinitely extended matter in equilibrium, for which one can derive theoretical results, and the situation in a collision where measurements are possible. That these theoretical predictions could have anything to do with quantities measurable in collisions is miraculous enough. It becomes more so if one looks at some distorting mechanisms in more detail.

A.1. *Temperature distributions.*

A.1.1 Primordial (due to velocity distributions). At all energies one finds rather flat rapidity distributions with a half-width larger than half the kinematic limit [47]. This proves that strong collective motions in the forward-backward direction survive the collision and that only a fraction of the totally available energy could have been thermalized. Therefore, a temperature distribution results such that at $y \approx 0$ we have $T \approx T_0$, while $T \Rightarrow 0$ when $|y| \to y_{max} \approx \ln(\sqrt{s}/m)$. This distribution will be different for different impact parameters b: in central collisions ($b \approx 0$) it will be flatter than in peripheral collisions, where it will be peaked at $y \simeq 0$.

A.1.2. Cooling. Particle emission and expansion will cause both, the quark-gluon plasma and the hadron gas, to cool [5]. However, most particles will be emitted during the hotter stages, because of the Boltzmann-type factors $\sim \exp[-m/T]$ entering in production rates.

A.1.3. The temperature distribution and measurable values. Let us combine all possible effects of this sort into a temperature distribution function $W(T; E, C_1, C_2, ...)$ which depends on the collision energy E and on experimental control parameters $C_1, C_2, ...$ (*e.g.*, acceptances, triggers, rapidity regions ...), but which is otherwise averaged over all collisions fulfilling these bias conditions at E; then, if X is a quantity whose expectation value $\langle X(T)\rangle$ can be calculated in the model at *fixed* T, its *experimental* value will be (if the model is correct)

$$\langle X\rangle_{expt} := \int W(T, E, ...)\langle X(T)\rangle \, dT \tag{A.1}$$

in particular for T itself

$$\langle T\rangle_{expt} := \int W(T, E, ...)\, T \, dT \tag{A.2}$$

and then in general

$$\langle X\rangle_{expt} \neq \langle X(\langle T_{expt}\rangle)\rangle \tag{A.3}$$

unless the control parameters $C_1, C_2, ...$ were chosen such that W is strongly peaked at some T (*e.g.*, by selecting $|y| \leqslant 1$, large multiplicities and/or heavy particles).

A.2. *Transverse collective motions.* – Already discussed in subsect. **3**·5. Hydrodynamic calculations [40-43] suggest nonnegligible transverse collective motions, which can broaden the local p_T distribution. The calculations having been done for heavy-ion collisions, little is known quantitatively about this effect in pp and $p\bar{p}$ collisions.

Expansion will have very much the same effect, but here again little is known.

A.3. *High cluster spin.* – High cluster spin was already discussed in subsect **3**·5; signatures [34]: *single* events should show azimuthal anisotropy with respect to the collision axis, large momenta and even a jet structure in and near some plane containing the collision axis, small momenta orthogonal to it. Averaged over events: an elongation of the p_T distribution towards larger p_T, hence larger p_T or larger apparent temperatures.

A.4. *Two-body decays.* – Heavy clusters do not explode at once into final particles, but disappear in steps along a decay chain, preferentially emitting in each step one or two (*) low-mass particles (π, K, $\mathcal{N}$) with low kinetic energy (of order T), so that in an average step the cluster mass decreases by only a few hundred MeV [48]. As long as the cluster mass is large compared to the emitted energy, the emitted particles have thermal distributions [37]. At the end of the decay chain as well as in the subsequent decay of some emitted resonant states (ρ, ω, Δ, ...) a two-body decay with *sharp* energy of the decay products will take place. This two-body decay is far from being thermal; what distorting effect will it have on the momentum distribution?

Let us assume the following situation: particles of mass m^* are emitted thermally with a Boltzmann distribution at temperature T. Then these particles decay: $m^* \to m_1 + m_2$ with fixed $m_{1,2}$ and, therefore, fixed momenta in the rest frame of m^*. What will be the averaged momentum distributions of m_1 and m_2 in the Lorentz frame where m^* had a thermal distribution? This problem is analytically solvable (ref. [49], subsect 7·6, and ref. [15], appendix IV) with the following results:

the spectral distributions of particles m_1 and m_2 will more or less differ from a pure Boltzmann distribution;

it, therefore, is, strictly speaking, not possible to assign to them a temperature; if one tries nevertheless by fitting them with a Boltzmann distribution, the resulting effective temperature is different from the original T and depends on the fit criteria (least square, same $\langle p \rangle$, same position of maximum); in view of the experimentally so easily accessible $\langle p_T \rangle$ the most reasonable method is a fit with a Boltzmann distribution having the same $\langle p \rangle$ as the particle considered. Our results below are computed this way.

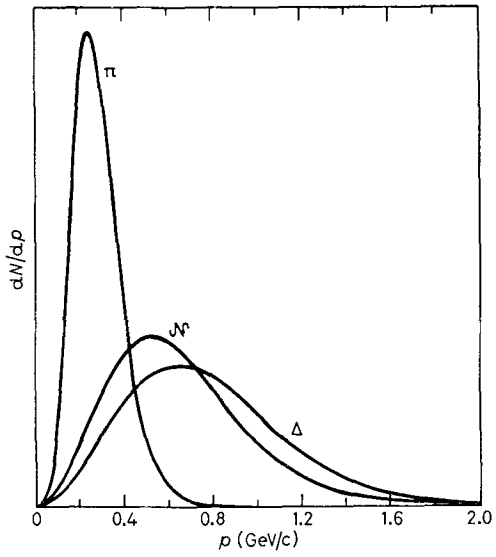

Fig. A.1. – The momentum distributions of the π and the $\mathcal{N}$ coming from the decay $\Delta \to \pi + \mathcal{N}$ when the Δ had a Boltzmann distribution with $T = 0.150$ GeV.

(*) Emission probabilities: $P(1):P(2):P(3) = 0.69:0.24:0.06$.

Example: decay $\Delta(1.23\ \text{GeV}) \to \mathcal{N}(0.94) + \pi(0.14)$; the Δ follows a Boltzmann distribution with $T = 0.150$ GeV.

Figure A.1 shows the three distributions (Δ, $\mathcal{N}$, π) as a function of the momentum p. Of course, π has much lower and $\mathcal{N}$ slightly lower momentum than Δ because of their masses. We now fit the curves for π and $\mathcal{N}$ of fig. A.1 with a Boltzmann function having the same $\langle p \rangle$ as the corresponding actual distributions. For $\mathcal{N}$ this works perfectly (fit and original indistinguishable within drawing accuracy; not shown here), $T_{\text{eff}}(\mathcal{N}) = 0.131$ GeV independently of the fit method; fig. A.2 shows that for the decay pion the « best Boltzmann » curve deviates rather much from the original (different fit procedures give

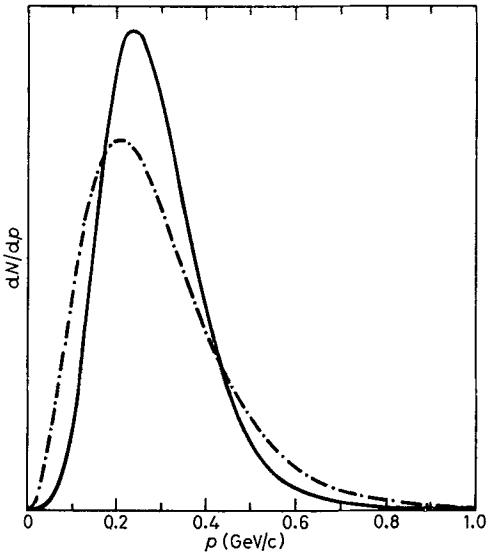

Fig. A.2. – The π momentum spectrum of fig. A.1 (———) fitted with a Boltzmann distribution (–·–·–) requiring that $\langle p \rangle_{\text{Boltzmann fit}} = \langle p \rangle_{\pi}$. While the Δ had a Boltzmann spectrum with $T = 0.150$ GeV, the Boltzmann fit to the daughter pion is rather bad; its temperature is 0.085 GeV.

visibly different results); the « same-$\langle p \rangle$ » method gives $T_{\text{eff}}(\pi) = 0.085$ GeV. (Least square: $T_{\text{eff}}(\pi) = 0.091$, « same maximum »: $T_{\text{eff}}(\pi) = 0.101$, hence differences of $\approx 15\,\%$.)

Of course, the pion with its smaller mass suffers more recoil than the nucleon and shows a more distorted spectrum.

Table A.I displays two cases in which the deviations (visible in the disagreement of the resulting T_{eff} from the three fits) of the spectra from thermal ones are reflected and two others proving the method to yield correct results in trivial cases.

The results in the last two lines are obvious: in line 3 nothing happens to the particle of mass 2 and in line 4 the two particles of mass 0.5 did not receive decay energy, hence they have a thermal spectrum with $T_{\text{eff}} = \frac{1}{2} T_{\text{original}}$ (the small differences in T_{eff} are due to our not having aimed at great numerical precision). The first two lines illustrate that the decay recoil can *lower as well as increase* the effective temperature; although in both cases the two daughter

TABLE A.I.

Decay (*)	$T_{original}$	T_{eff} same maximum	T_{eff} same $\langle p \rangle$	T_{eff} least square	Remarks about momentum spectrum
$\pi^0 \to 0 + 0$	0.150	0.034	0.082	0.063	far from thermal
$2 \to 0 + 0$	0.190	0.500	0.386	0.440	far from thermal
$2 \to \underline{2} + 0$	0.190	0.190	0.189	0.187	exactly thermal (trivial)
$1 \to 0.5 + 0.5$	0.190	0.095	0.095	0.094	exactly thermal (trivial)

(*) The numbers give the masses in GeV.

particles have zero mass, the effect is opposite in the two cases; the high T_{eff} in the second case is simply borrowed from the large parent mass. Since no general rule (except for the unhandy analytic formulae [15]) can be given, we have computed several realistic examples and obtained more or less satisfactory Boltzmann fits (always «same $\langle p \rangle$»).

The results for $\rho \to \pi\pi$, $\Delta \to (\underline{\mathcal{N}}\pi$ and $\mathcal{N}\underline{\pi})$ and $\pi_0 \to \gamma\gamma$ are summarized in terms of effective temperatures as functions of the original temperature $T_{original}$ at which the parent particle was emitted (*) (fig. A.3). The broken line $T = T_{original}$ illustrates well what distortions in effective temperature (determined from $\langle p_T \rangle$) we have to envisage from 2-body decays. As mentioned

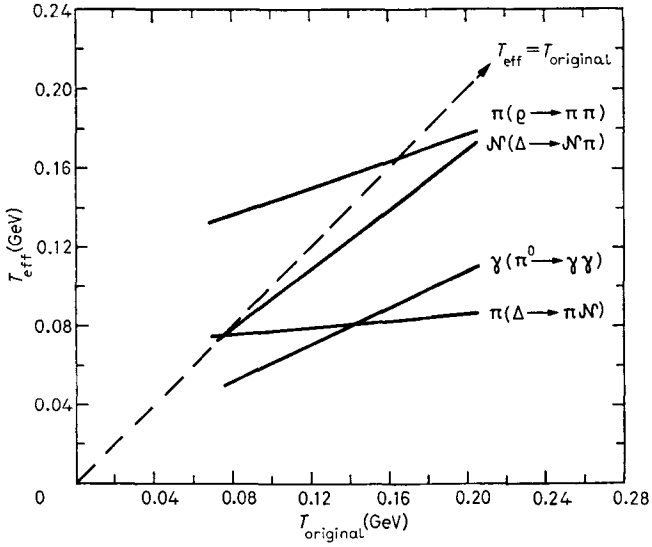

Fig. A.3. – The effective temperatures T_{eff} of the daughter particles in a few typical decays plotted against the temperature belonging to the Boltzmann distribution of the parent particle $T_{original}$ (from Boltzmann fit requiring $\langle p \rangle_{fit} = \langle p \rangle_{original}$).

(*) The relation $T_{eff} = f(T_{original}, m^*, m_1, m_2)$ is linear within drawing accuracy in the region $0.1 \text{ GeV} \leqslant T_{original} \leqslant 0.2$ GeV. As this is the only interesting region, we did not try to find how T_{eff} behaves outside it.

above, such decays occur mostly at the end of decay chains and occasionally if a cluster emits a resonance which dominatingly decays into two stable particles. Thus in very-high-energy collisions the contribution of genuine 2-body decays may be small and the distortion too; its general trend will be to lower the apparent temperature.

A.5. *Contributions from the quark gluon phase.* – We have stated that fig. 4.1 suggests that about once in 600 ordinary events (hadronization at the phase transition) a leakage from the quark gluon plasma occurs; from ISR to UA1 this fraction does not much depend on the collision energy. What then is the influence on $\langle p_T \rangle$ from the tails? Assume for simplicity that the distribution is given by the sum of the ordinary plus a leakage contribution and that, therefore (neglecting for this order-of-magnitude estimate the influence of masses),

$$\frac{\mathrm{d}(\mathrm{d}N/\mathrm{d}y)}{2\pi p_\perp \,\mathrm{d}p_\perp} \approx A_{\mathrm{low}} \exp\left[-p_\perp/T_{\mathrm{low}}\right] + A_{\mathrm{high}} \exp\left[-p_\perp/T_{\mathrm{high}}\right]. \tag{A.4}$$

Then

$$\langle p_\perp \rangle = \langle p_\perp \rangle_{\mathrm{low}} \frac{1 + (A_{\mathrm{high}}/A_{\mathrm{low}})(T_{\mathrm{high}}/T_{\mathrm{low}})^3}{1 + (A_{\mathrm{gigh}}/A_{\mathrm{low}})(T_{\mathrm{high}}/T_{\mathrm{low}})^2}. \tag{A.5}$$

With $A_{\mathrm{high}}/A_{\mathrm{low}} = 1/600$ we obtain for the correction factor the values displayed in fig. A.4; for UA1 this amounts to an increase by $\sim 15\,\%$, while for ISR it

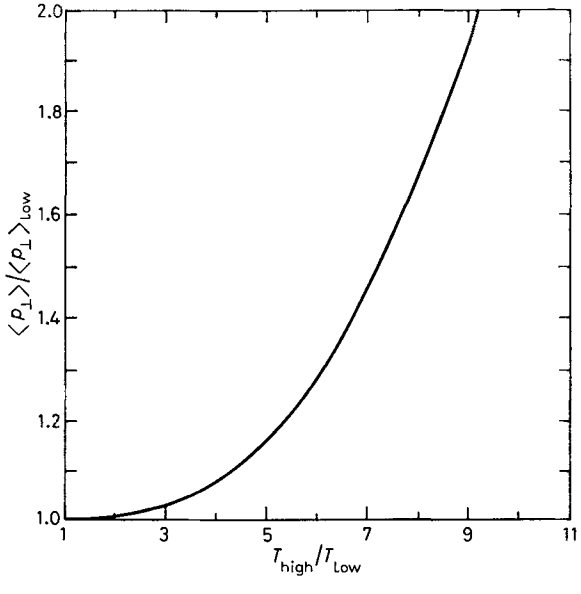

Fig. A.4. – This figure illustrates that the $\langle p_T \rangle$ resulting from the superposition $f(p_T) = A_{\mathrm{low}} \exp\left[-p_T/T_{\mathrm{low}}\right] + A_{\mathrm{high}} \exp\left[-p_T/T_{\mathrm{high}}\right]$ is even for $A_{\mathrm{high}} \ll A_{\mathrm{low}}$ (here 1:600) substantially larger than the $\langle p_T \rangle_{\mathrm{low}}$ resulting from the low-T component alone. This effect would amount to an increase of 1 to 3% at ISR and $\approx$ 15% at the Collider. Though it contains few particles, the large-p_T tail does influence $\langle p_T \rangle$ significantly. Our figure gives a lower limit.

remains of the order of 1 to 3%. Thus the influence of the tail alone can raise the $\langle p_T \rangle$ from ≈ 0.40 GeV/c at ISR to ≈ 0.46 GeV/c at UA1; this effect almost explains the difference in the limiting values of $\langle p_T \rangle$ for large multiplicities in the two experiments.

This is, however, a qualitative statement, because in reality one needs at least a superposition of three exponentials (*) to fit the experimental p_T distributions including the tails. Also, as shown in appendix B, $\exp[-p_T/T]$ is not a very good ansatz for determining $\langle p_T \rangle$; in this estimate, however, a good part of the latter error cancels on both sides in eq. (A.5).

A.6. *Imperfect equilibrium even locally.* – This is very difficult to estimate; should it happen that hadron matter in very-high-energy collisions is always very far from local equilibrium, our whole method would become inapplicable (**). That it nevertheless gives reasonable results can be taken as an indication that local equilibrium is more or less reached. Still, one has to distinguish between *kinetic* and *chemical* equilibrium, the approach to the latter depending on individual coupling strength and/or cross-sections [28]. It can happen that it makes sense to speak of a local temperature, but that ratios of particle numbers for different species are still far from their equilibrium values at that temperature.

A.7. *Summary of distortive mechanisms.* – The various effects discussed (with the exception of the last, which is beyond control) may partly compensate each other. We put them together in table A.II, which may explain

TABLE A.II.

Effect on apparent temperature	$T_{\text{eff}} > T_{\text{original}}$	$T_{\text{eff}} < T_{\text{original}}$
temperature distribution due to collective motion and cooling	no	yes
transverse collective motion	depends on kinematics	
cluster spin	yes	no
2-body decay	yes at low T_{original}	yes at high T_{original}
leakage from the quark-gluon phase	yes	no

why the experimental values for T_0 given in the literature vary between 0.14 GeV and 0.20 GeV.

It must be stressed that none of the mentioned distorting mechanisms could possibly simulate a phase transition when it was not there, nor could they hide it, if it is there.

(*) Cooling; see subsect. 4·5.

(**) Even nonequilibrium statistical thermodynamics would then not help, because it uses the concept of local temperature.

APPENDIX B

Difficulties in determining p_T.

In high-energy hadron physics the p_T distribution is strongly decreasing: for p_T up to about $(1 \div 2)$ GeV/c nearly exponentially and then like a high power of $1/p_T$ (or as a superposition of exponentials with smaller $1/T$). It is, therefore, obvious that the region of small p_T contributes dominantly to $\langle p_T \rangle$; as the current $\langle p_T \rangle$ are of order 0.5 GeV/c, the region below 0.5 GeV/c gives the main contributions. Unfortunately, it is difficult to measure p_T down to zero in very-high-energy experiments. Therefore, there are often cuts in the data excluding all p_T below, say, 0.15 to 0.3 GeV/c (that is, excluding the most important part contributing to $\langle p_T \rangle$). It is then customary to fit the measurable p_T distribution—often over a very large region up to several GeV/c—with some function, which then, if the fit is good, is extrapolated to zero and $\langle p_T \rangle$ computed from it. Such a procedure appears reasonable if looked at in a logarithmic plot, but it may induce considerable errors, because the usually taken fit functions (looking so nice over large intervals) happen to fail seriously just in the region into which they are extrapolated and which is the most important one for $\langle p_T \rangle$: namely, below 0.3 to 0.5 GeV/c, where, as we shall see, the (most likely) true distributions have a Gaussian shape which is not reproduced by most fit functions.

The aim of this appendix is to illustrate what are the systematic errors possibly introduced by computing $\langle p_T \rangle$ from these fits. While we shall show as examples the distributions for the π, K and $\mathcal{N}$ mass, the experimental situation is most often such that the p_T distribution is measured for a mixture of unidentified particles. We, therefore, give also such an example where $\pi+\mathrm{K}+\mathcal{N}$ are superimposed. Finally, we show the dangers in using a nice-looking semi-empirical formula.

B.1. *The most likely true distributions at low p_T and their corresponding $\langle p_T \rangle$.* – The claim of all statistical models (whatever their degree of sophistication) that below $p_T \approx 1$ GeV/c the inclusive p_T distribution should be roughly thermal has never been falsified; at lower energies it has been explicitly confirmed; it has even been shown that pions obey a Bose-Einstein-Planck distribution [50, 51]. We cannot reasonably doubt that this will remain true at ISR and collider energies, where with the higher energy density the number of degrees of freedom increases and, therefore, the thermodynamical description should become still more adequate.

In this appendix, we, therefore, *assume that the p_T distribution below $p_T \sim 1$ GeV/c is thermal.* This is a safe assumption in the central rapidity region $(-1 \leqslant y \leqslant 1)$; it might be true even up to the ends.

From an isotropic thermal distribution of particles with mass m at temperature T, one derives by integrating over an arbitrary «longitudinal» direction [23, 24] the p_T distribution

$$\text{(B.1)} \qquad W(p_\perp)\,\mathrm{d}p_\perp = \text{const}\cdot \mathrm{d}p_\perp p_\perp \sqrt{p_\perp^2 + m^2} \sum_{n=1}^{\infty} (\mp 1)^{n+1} K_1\left(n \frac{\sqrt{p_\perp^2 + m^2}}{T}\right),$$

where $\{\mp 1\} \Leftrightarrow \{\text{fermions/bosons}\}$.

This formula remains unchanged if collective motions in only one direction (« longitudinal ») exist and when T does not (or very little) depend on the longitudinal velocity [23], as is indeed the case over large parts of the rapidity distribution (see subsect. 1·2). We thus have good reasons to assume this formula to be true for most particles produced.

Note that $W(p_T)$ is defined above such that

$$\int W(p_\perp)\,\mathrm{d}p_\perp \sim \text{number of particles} \tag{B.2}$$

that is, the phase-space factor $2\pi p_T$ is absorbed into $W(p_T)$. We rewrite (B.1) to conform with the currently used notation. Using

$$E\frac{\mathrm{d}^3\sigma}{\mathrm{d}p^3} \equiv E\frac{\mathrm{d}^3\sigma}{2\pi p_\perp \mathrm{d}p_\perp \mathrm{d}p_\parallel} \tag{B.3}$$

and introducing the rapidity y

$$\begin{cases} p_\parallel = \sqrt{p_\perp^2 + m^2}\sinh y\,, \\ E = \sqrt{p_\perp^2 + m^2}\cosh y\,, \\ E^2 = p_\perp^2 + p_\parallel^2 + m^2\,, \end{cases} \tag{B.4}$$

we find $\mathrm{d}p_\parallel = E\,\mathrm{d}y$, so that

$$E\frac{\mathrm{d}^3\sigma}{\mathrm{d}p^3} = \text{const}\cdot\frac{1}{2\pi p_\perp}\frac{\mathrm{d}(\mathrm{d}N/\mathrm{d}y)}{\mathrm{d}p_\perp} \tag{B.5}$$

with $\mathrm{d}N/\mathrm{d}y$ being the total multiplicity per unit rapidity of the species (mass m) considered. Normalization does not interest here, hence

$$\begin{aligned} \frac{1}{2\pi p_\perp}\frac{\mathrm{d}(\mathrm{d}N/\mathrm{d}y)}{\mathrm{d}p_\perp} = \text{const}\cdot\frac{W(p_\perp)}{p_\perp} = \text{const}\cdot E\frac{\mathrm{d}^3\sigma}{\mathrm{d}p^3} = \\ = \text{const}\cdot\sqrt{p_\perp^2 + m^2}\sum_{n=1}^{\infty}(\mp 1)^{n+1}K_1\left(n\frac{\sqrt{p_\perp^2 + m^2}}{T}\right). \end{aligned} \tag{B.6}$$

From this the mean p_T becomes

$$\langle p_\perp(m, T)\rangle = \frac{\int p_\perp(\mathrm{d}(\mathrm{d}N/\mathrm{d}y)/2\pi p_\perp \mathrm{d}p_\perp)\,2\pi p_\perp \mathrm{d}p_\perp}{\int(\mathrm{d}(\mathrm{d}N/\mathrm{d}y)/2\pi p_\perp \mathrm{d}p_\perp)\,2\pi p_\perp \mathrm{d}p_\perp}. \tag{B.7}$$

The integrations can be done with the result [23, 24]

$$\langle p_\perp(m, T)\rangle_{\substack{\text{Fermi}\\\text{Bose}}} = \sqrt{\frac{\pi m T}{2}}\frac{\sum_{n=1}^{\infty}(\mp 1)^{n+1}K_{\frac{3}{2}}(n(m/T))}{\sum_{n=1}^{\infty}(\mp 1)^{n+1}K_2(n(m/T))}. \tag{B.8}$$

Equations (B.6), (B.8) are the official, model-independent expressions for the p_T distribution and for $\langle p_T \rangle$ when thermalization at fixed temperature T is assumed. Models differ by using different equations of state, *i.e.* relations between energy density, temperature and chemical potential(s).

B.2. *Comparison to two approximations.* – We now compare these exact formulae numerically with two frequently used approximations:

$$\frac{\mathrm{d}(\mathrm{d}N/\mathrm{d}y)}{2\pi p_\perp \mathrm{d}p_\perp} \approx \begin{cases} \exp\left[-p_\perp/T\right], \\ \exp\left[-\sqrt{p_\perp^2 + m^2}/T\right], \end{cases} \tag{B.9}$$

in the case of Bose, Boltzmann ($n = 1$ in (B.6), (B.8)) and Fermi statistics at several mass values (though to each mass belongs a definite quantum statistics, we compare with all; *e.g.*, for fake π fermions). Note that the second choice of (B.9) really covers also the first; in fact,

$$\exp\left[-\sqrt{p_\perp^2 + m^2}/T\right] \begin{cases} \sim \exp\left[-p_\perp^2/2mT\right] & \text{for } p_\perp \ll m, \\ \sim \exp\left[-p_\perp/T\right] & \text{for } p_\perp \gg m, \end{cases} \tag{B.10}$$

thus it also covers the sometimes used Gaussian approximation. Indeed, if one neglects quantum statistics (Bose, Fermi) and assumes that $m/T \gg 1$, then from $K(x) \sim \sqrt{\pi/2x} \exp\left[-x\right]$ $(x \gg 1)$ it follows that eq. (B.6) becomes [23]

$$\frac{\mathrm{d}(\mathrm{d}N/\mathrm{d}y)}{2\pi p_\perp \mathrm{d}p_\perp} \underset{m/T \gg 1}{\Rightarrow} \mathrm{const} \cdot (p_\perp^2 + m^2)^{\frac{1}{2}} \exp\left[-\sqrt{p_\perp^2 + m^2}/T\right], \tag{B.11}$$

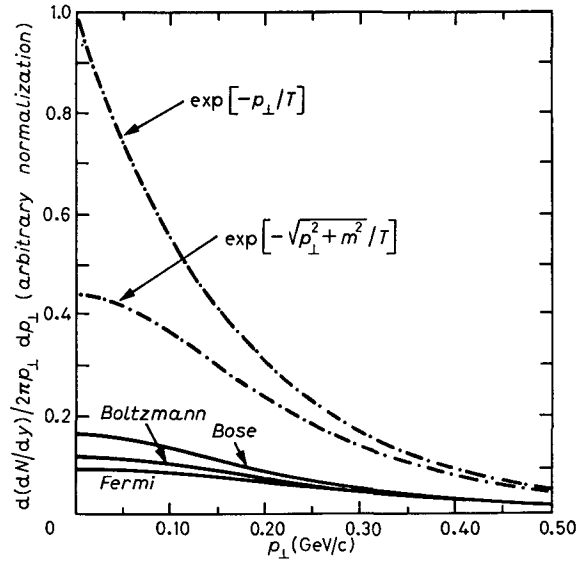

Fig. B.1. – Thermal p_T distributions (of π). The three exact curves (Bose, Boltzmann, Fermi) are compared to $\exp\left[-\sqrt{p_T^2 + m}/T\right]$ and $\exp\left[-p_T/T\right]$ for $m = m_\pi$; $T = 0.167$ GeV, over a small p_T interval in a linear plot.

where, of course, the exponential is the most varying part. We conclude from (B.11) that, *if drastic approximations must be made,* $\exp[-\sqrt{p_T^2 + m^2}/T]$ *not only covers the Gaussian and the linear exponential, it also is the physically best motivated one* [52]. If only p_T but no masses are measured, one might take m and T as fit parameters and will, up to $p_T \approx 1$ GeV, obtain something much better than with either Gaussian or linear exponential fits (*).

Our comparisons are made at $T = 0.167$ GeV.

Figures B.1 and B.2 show the distributions at the pion mass; once linearly over a small interval and once logarithmically over a larger one; the second figure shall only illustrate how misleadingly nice things can look in a logarithmic scale.

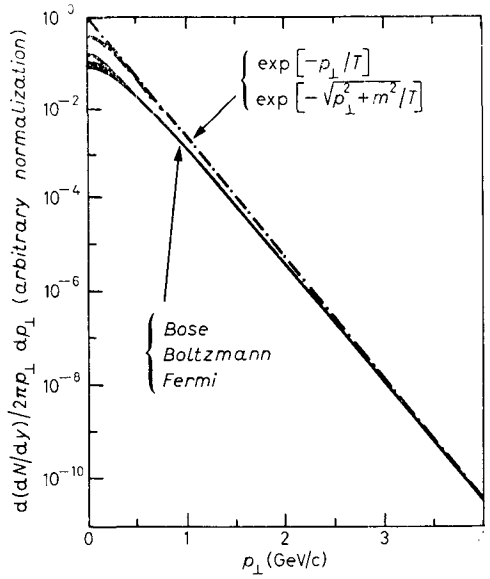

Fig. B.2. – The same p_T distribution (of π) as fig. B.1, but over a large p_T interval in a logarithmic plot. The enormous differences in the most important low-p_T region are less exhibited than in fig. B.1.

For the nucleon mass (fig. B.3 and B.4), the effect of quantum statistics is negligible, but $\exp[-p_T/T]$ is really bad.

Next, we compare the $\langle p_T \rangle$ values following from these approximations:

(B.12)
$$\begin{cases} \text{exact:} & \text{(eq. B.8)}\,; \\ \text{Boltzmann:} & \langle p_\perp \rangle = \sqrt{\dfrac{\pi m T}{2}}\,\dfrac{K_{\frac{3}{2}}(m/T)}{K_2(m/T)}\,; \\ \exp[-p_\perp/T]\text{:} & \langle p_\perp \rangle = 2T\,; \\ \exp[-\sqrt{p_\perp^2 + m^2}/T]\text{:} & \langle p_\perp \rangle = \sqrt{\dfrac{\pi m T}{2}}\,\dfrac{K_2(m/T)}{K_{\frac{3}{2}}(m/T)}\,. \end{cases}$$

(*) I have been trying to progapate this simple consideration for about 15 years; it seems to be in vain.

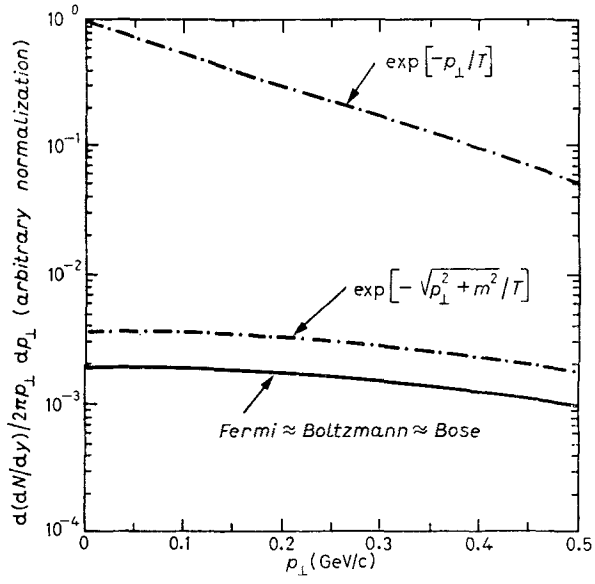

Fig. B.3. – p_T distributions as in fig. B.1, but for the nucleon. With the larger nucleon mass the differences between the exact and approximate formulae are more pronounced; statistics, however, is unimportant.

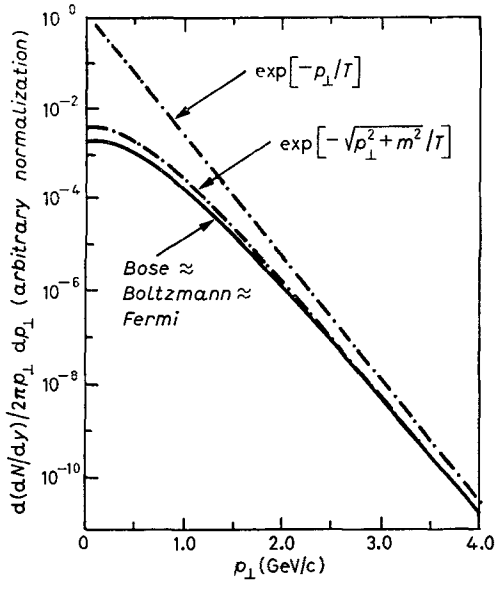

Fig. B.4. – p_T distributions as in fig. B.2, but for the nucleon. With the larger nucleon mass the differences between the exact and approximate formulae survive in the logarithmic plot over a large interval: statistics, however, is unimportant.

Consider first the limiting cases $m/T \to 0, \infty$:

$m/T \to 0$

$$\text{(B.13)} \qquad \begin{cases} \langle p_\perp \rangle_{\substack{\text{Fermi} \\ \text{Bose}}} \Rightarrow \dfrac{3\pi}{4} T \dfrac{\zeta(\frac{5}{2})}{\zeta(2)} \begin{Bmatrix} 2 - \frac{1}{2}\sqrt{2} \\ 1 \end{Bmatrix} = T \begin{Bmatrix} 2.483 \\ 1.921 \end{Bmatrix}, \\ \langle p_\perp \rangle_{\text{Boltzmann}} \Rightarrow \dfrac{3\pi}{4} T = 2.356 T, \\ \langle p_\perp \rangle_{\exp[-p_\perp/T]} \Rightarrow \langle p_\perp \rangle_{\exp[-\sqrt{p_\perp^2 + m^2}/T]} \Rightarrow 2T. \end{cases}$$

For $m \to 0$, the last two members of eq. (B.12) must obviously become equal.

$m/T \to \infty$

$$\text{(B.14)} \qquad \begin{cases} \langle p_\perp \rangle_{\text{exact}} \Rightarrow \langle p_\perp \rangle_{\text{Boltzmann}} \Rightarrow \langle p_\perp \rangle_{\exp[-\sqrt{p_\perp^2 + m^2}/T]} \Rightarrow \sqrt{\dfrac{\pi m T}{2}}, \\ \langle p_\perp \rangle_{\exp[-p_\perp/T]} = 2T. \end{cases}$$

We show the distributions (B.12) in the most usual temperature interval $0.1\ \text{GeV} \leqslant T \leqslant 0.2\ \text{GeV}$ in fig. B.5-B.7.

The lesson from these figures is that statistics is still important for $\langle p_T \rangle_\pi$, while for K and $\mathcal{N}$ it may be safely neglected. In all cases $\exp[-\sqrt{p_T^2 + m^2}/T]$ induces an underestimate of $\langle p_T \rangle$ by 4 to 7%, while $\exp[-p_T/T]$ leads to values too low by 12 to 45%. Thus the latter should really never be used for extrapolations aiming at determining $\langle p_T \rangle$.

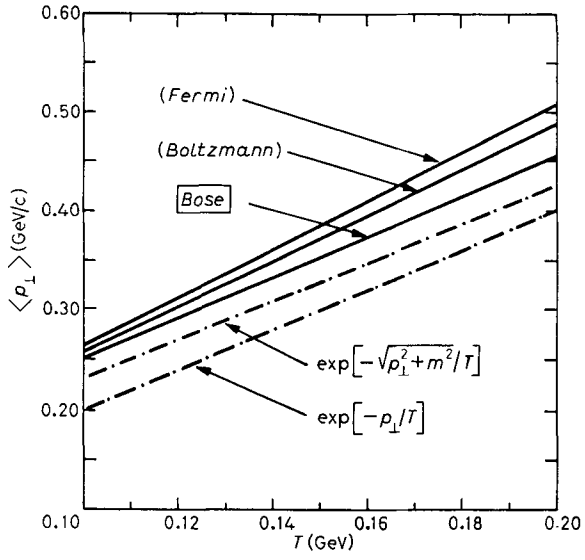

Fig. B.5. – Mean transverse momenta computed from exact (B.8) and approximate formulae (B.12) for π; $\exp[-p_T/T]$ gives inacceptably bad estimates of $\langle p_T \rangle$.

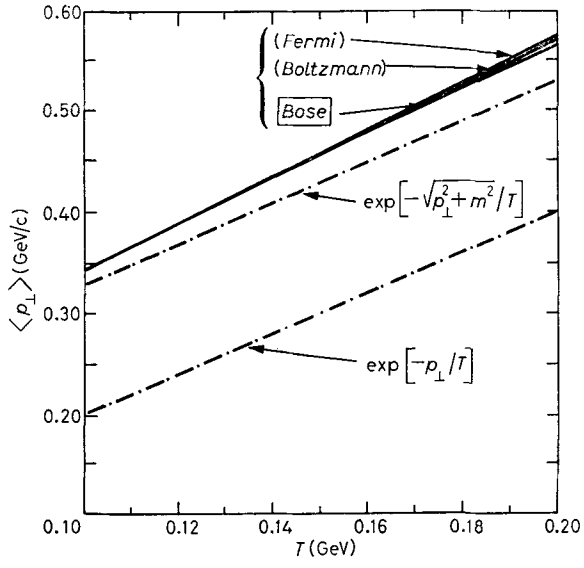

Fig. B.6. – Mean transverse momenta computed from exact (B.8) and approximate formulae (B.12) for K. Already for K statistics is a 1% effect; $\exp[-p_T/T]$ gives inacceptably bad estimates of $\langle p_T \rangle$.

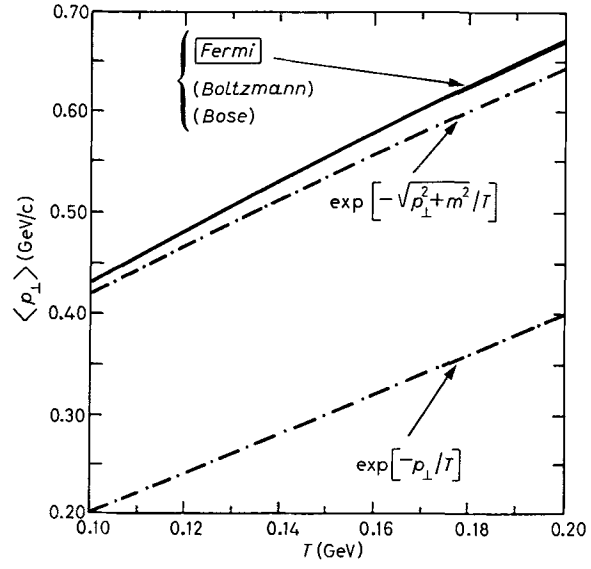

Fig. B.7. – Same as fig. B.5 and B.6, but for $\mathcal{N}$.

Next, we compare $\exp[-p_T/T]$ to a reasonably realistic superposition $\pi+K+\mathcal{N}$. While in the previous examples we have compared the «true» and approximate distributions *at the same* T, we now change the philosophy:

we calculate from the exact eq. (B.6) a superposition of $80\,\%\,\pi + 15\,\%\,K + 5\,\%\,\mathcal{N}$ at $T = 0.15$ GeV and assume this distribution to be a

realistic one up to $p_T = 1.5$ GeV/c. We give this «fake experimental» distribution to someone to fit it with $A \exp[-p_T/T]$ over various intervals (p_T cuts) with A and T as free parameters and see what happens.

Fit 1:	$0 \text{ GeV/c} \leqslant p_T \leqslant 1.5 \text{ GeV/c}$,	no cut,
fit 2:	$0.3 \text{ GeV/c} \leqslant p_T \leqslant 1.5 \text{ GeV/c}$,	lower cut,
fit 3:	$0.3 \text{ GeV/c} \leqslant p_T \leqslant 1 \text{ GeV/c}$,	lower and upper cut;

the lower cut is not unusual [4] in high-energy experiments; the upper one might have been motivated by trying to avoid the influence of the large-p_T component. The belief in $\exp[-p_T/T]$ as a good representation of data is, of course, due to usually plotting p_T distributions logarithmically over a large p_T range and cutting them below (0.1 to 0.3 GeV/c). Then they look indeed suitable for such a procedure. Moreover, this optical illusion may seduce one to fit the *logarithm* of the distribution with $a + bp_T$. This is what we have done in this example, whose result is displayed in fig. B.8 (fit 1), B.9 (fit 2) and B.10 (fit 3); to

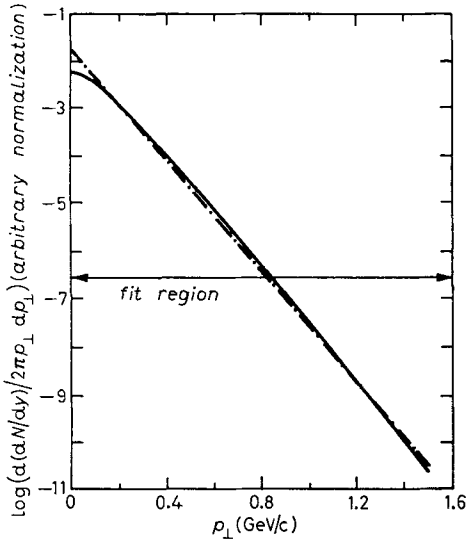

Fig. B.8. – The full line represents a «fake experimental» distribution: superposition of 80% π + 15% K + 5% $\mathcal{N}$ with $T = 0.15$ GeV computed from the exact formula (B.6); the broken line is a best fit to the logarithm with $a + bp_T$ in the region $0 \text{ GeV} \leqslant p_T \leqslant 1.5$ GeV/c (fit 1).

see how good the fits look, one should cover in fig. B.9, B.10 the excluded part with a strip of paper. How bad it really is if used as an extrapolation to determine $\langle p_T \rangle$ is shown in a linear plot in fig. B.11. Depending on the fit region we obtain different estimates of T and $\langle p_T \rangle$ as listed in table B.I.

All $\langle p_T \rangle_{\text{fit}}$ are too low by about 10%, while differing among each other by $\sim 3\%$; the temperature is estimated too high by 10 to 15%.

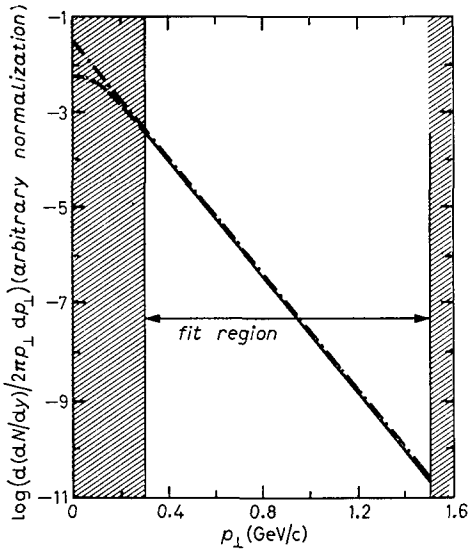

Fig. B.9.

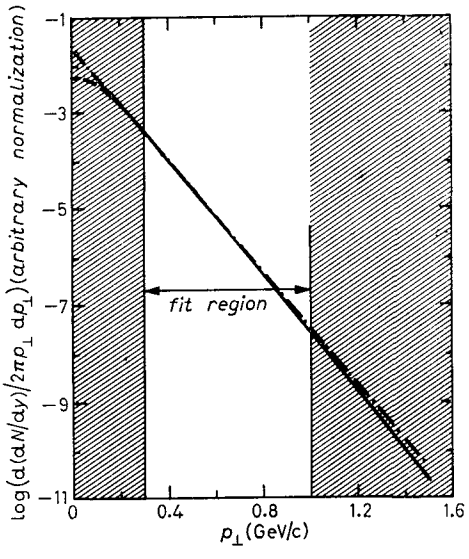

Fig. B.10.

Fig. B.9. – The same as fig. B.8 but with a different fit interval: $0.3 \leqslant p_\perp \leqslant 1.5$ (fit 2). Fit 2 looks much better than fit 1, provided one regards only the fit interval.

Fig. B.10. – The same as fig. B.8 but with a different fit interval: $0.3 < p_\perp < 1$ (fit 3). Fit 3 is almost perfect, provided one regards only the fit interval (assume data for $p_T \leqslant 0.3$ GeV/c unknown; cover the regions outside the fit interval with a piece of paper).

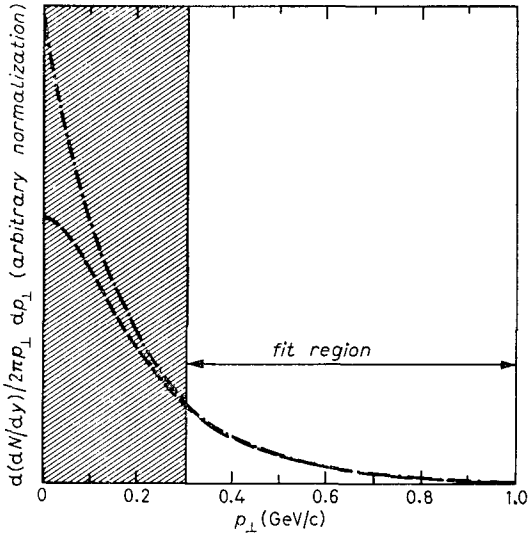

Fig. B.11. – Same as fig. B.10 but in a linear plot; if only the fit region is considered even here the fit is perfect. If used for computing $\langle p_T \rangle$ it would, however, give a bad result, as obvious from the shaded part.

TABLE B.I. – *Fit of a «fake experimental» p_T distribution with* $\exp[-p_T/T]$.

Fit region	T_{fit}	$\langle p_T \rangle_{fit}$	« true values »
fit 1			
$0 \leqslant p_T \leqslant 1.5$	0.171	0.342	
fit 2			$T = 0.150$
$0.3 \leqslant p_T \leqslant 1.5$	0.166	0.333	$\langle p_T \rangle = 0.378$
fit 3			
$0.3 \leqslant p_T \leqslant 1$	0.171	0.34	

B.3. *An empirical formula inspired by* QCD. – The previous examples were restricted to $p_T \leqslant 1.5$ GeV/c. This is the main region contributing to $\langle p_T \rangle$.

We know, however, that above 1.5 GeV/c the distribution becomes flatter due to the large p_T which may push up $\langle p_T \rangle$ by order of 10 % (appendix A.5). It is then tempting to try to fit the whole distribution (which may have a cut at low p_T) with one single expression inspired by QCD; for instance with

$$E\frac{d^3\sigma}{dp^3} = \text{const}\cdot\frac{d(dN/dy)}{2\pi p_\perp dp_\perp} = A\left(\frac{p_0}{p_\perp + p_0}\right)^n, \tag{B.15}$$

which—over a large p_T interval 0.3 GeV/c $\leqslant p_T \leqslant$ 10 GeV/c and plotted logarithmically—gives indeed an impressive fit (see fig. 1.3) [4], seducing one to compute also $\langle p_T \rangle$ from it. This will induce again systematic errors of the order of 10 % and more. Indeed, for $p_T \to 0, \infty$, we have

$$\left(\frac{p_0}{p_\perp + p_0}\right)^n \begin{cases} 1 - \dfrac{n}{p_0} p_\perp \approx \exp\left[-\dfrac{n}{p_0} p_\perp\right] & \text{for } p_\perp \to 0, \\ \left(\dfrac{p_0}{p_\perp}\right)^n & \text{for } p_\perp \to \infty. \end{cases} \tag{B.16}$$

Just in the most important small-p_T region, this distribution approaches the simple exponential with all its disadvantages (table B.I).

Thus in spite of the impressive fit, which now includes the large p_T, the estimate of $\langle p_T \rangle$ coming from it

$$\langle p_\perp \rangle = \frac{\int (p_0/(p_\perp + p_0))^n p_\perp^2 \, dp_\perp}{\int (p_0/(p_\perp + p_0))^n p_\perp \, dp_\perp} = \frac{2p_0}{n-3}, \tag{B.17}$$

will be ~10 % too low—an error of the order of the ISR/UA1 discrepancy at low multiplicities (fig. 1.1).

The semi-empirical distribution (B.15) suffers, however, from a further, equally important disease: its nonuniqueness. Indeed, the « same » curve (within about experimental errors) can be obtained with rather different parameters yielding $\langle p_T \rangle$ differing by up to 10 %. This is illustrated in the following example: we draw the three curves listed in table B.II and plotted in fig. B.12.

TABLE B.II. – *Three curves of the type* $(p_0/(p_0 + p_T))^n$

p_0 (GeV/c)	n	$\langle p_T \rangle = 2p_0/(n-3)$ (GeV/c)
1.0	8	0.400
1.3	9	0.433
1.6	10	0.457

The lesson is that eq. (B.15) is unsuitable for determining $\langle p_T \rangle$ from the data, because its inherent nonuniqueness as well as its failing at low p_T introduce errors of the order of 10% which may compensate, or add up to 20%.

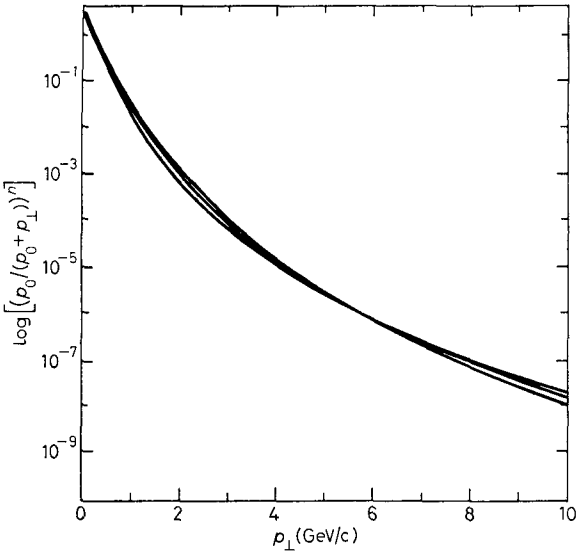

Fig. B.12. – The essential nonuniqueness of fits with $(p_0/(p_0 + p_T))^n$. The three curves belong to three different sets of parameters

$$\begin{Bmatrix} p_0 \\ n \end{Bmatrix} = \begin{Bmatrix} 1.0 \\ 8 \end{Bmatrix} \begin{Bmatrix} 1.3 \\ 9 \end{Bmatrix} \begin{Bmatrix} 1.6 \\ 10 \end{Bmatrix}$$

and deviate from each other by about typical experimental errors. Yet they give $\langle p_T \rangle = 0.400$, 0.433, 0.457 GeV/c (mainly due to their different slopes at $p_T = 0$). To this adds the error common to all fits approaching an exponential at $p_T \to 0$. (See fig. B.11 and table B.I.)

B.4. *A better fit method for finding* $\langle p_T \rangle$. – Neither the thermodynamic formula (B.6) nor the power law (B.15) can be used to determine $\langle p_T \rangle$, because the first does not reproduce the tail at large p_T (which can contribute $\approx 15\%$ to $\langle p_T \rangle$, see subsect. A.5), while the second fails to account for the flattening at $p_T = 0$ (whereby $\langle p_T \rangle$ may be underestimated by $\approx 10\%$). As, however, their ranges of validity seem to overlap in the region 0.5 to 1 GeV/c, one might expect a good fit over all p_T with a suitable combination of the two; $\langle p_T \rangle$ cal-

culated from this would be a safe estimate including the influence of the large p_T as well as that of the Gaussian-type flattening at $p_T = 0$.

I propose the following method:

find $N_\pi : N_K : N_N : N_Y$ from experiment or by extrapolation or from a model; a rough guess is sufficient;

fit the experimental distribution with

$$\text{(B.18)} \quad f(p_\perp) := A \cdot \theta(p_1 - p_\perp) \left\{ \sum_{i=\pi,K,\ldots} N_i \sqrt{p_\perp^2 + m_i^2} \sum_{l=1}^{l_{\max}} (\mp 1)^{l+1} K_1 \left(l \frac{\sqrt{p_\perp^2 + m_i^2}}{T} \right) \right\} +$$

$$+ B\theta(p_\perp - p_1) \left(\frac{p_0}{p_\perp + p_0} \right)^n ,$$

$$\theta(x) \text{ is the usual step function, } (\mp 1) \equiv \begin{cases} \text{fermions} \\ \text{bosons} \end{cases},$$

where the N_i are given and where the switching point p_1 may be chosen anywhere between 0.5 and 1 GeV/c (as seen from fig. B.9-B.11, the fit should not significantly depend on this choice), while the fit parameters are A, B, T, p_0 and n. One then requires that at p_1 values and slopes of the two functions should match, which leaves one with only 3 free parameters, say A, T, n. This method should suffer little from the nonuniqueness encountered with the power fit (B.15) (fig. B.12 and table B.II), since T would essentially depend on the thermal part, n on the tail and A on the overall normalization.

The sum over l (coming from Bose/Fermi statistics) can be cut off at $l_{\max} = 10$ for pions, at 5 for kaons and at 1 for nucleons and hyperons (see fig. B.1, B.4). The whole procedure would, even on a small computer, take not much more time that the fit with eq. (B.15) alone; it would, however, give a much safer estimate of $\langle p_T \rangle$ in all cases where a lower cut in the data makes its direct determination impossible.

I suspect that, if the collider *and* ISR data are analysed with this method, the apparent inconsistency visible in fig. 1.1 will be reduced (if it will not disappear altogether).

REFERENCES

[1] H. SATZ, Editor: *Statistical Mechanics of Quarks and Hadrons, Proceedings of the International Symposium, Bielefeld, 1980* (North Holland, Amsterdam, 1981).

[2] M. JACOB and H. SATZ, Editors: *Quark Matter Formation and Heavy-Ion Collisions, Proceedings of the Bielefeld Workshop, 1982* (World Scientific, Singapore, 1982). See also M. JACOB and J. TRAN THANH VAN: *Phys. Rep.*, **88**, 321 (1982).

[3] *a*) AMES-BOLOGNA-CERN-DORTMUND-HEIDELBERG-WARSAW COLLABORATION: *Multiplicity dependence of transverse momentum spectra at* ISR *energies*, contribution to the *Europhysics International Conference on High-Energy Physics, Brighton (UK), 1983* (CERN preprint EP/1456R/WG/mk); *b*) M. A. FASSLER: *Nucl. Phys. A*, **400**, 525c (1983); *c*) THE AXIAL FIELD SPECTROMETER COLLABORATION: *Phys. Lett. B*, **119**, 464 (1982).

[4] UA1 COLLABORATION: *Phys. Lett. B*, **118**, 167 (1982).

[5] R. HAGEDORN and J. RAFELSKI: *Phys. Lett. B*, **97**, 136 (1980).
[6] R. HAGEDORN and J. RAFELSKI: in *Statistical Mechanics of Quarks and Hadrons, Proceedings of the International Symposium, Bielefeld, 1980* (North Holland, Amsterdam, 1981), p. 237.
[7] J. RAFELSKI and R. HAGEDORN: in *Statistical Mechanics of Quarks and Hadrons, Proceedings ot the International Symposium, Bielefeld, 1980* (North Holland, Amsterdam, 1981), p. 253.
[8] R. HAGEDORN: *Z. Phys. C*, **17**, 265 (1983).
[9] R. HAGEDORN, I. MONTVAY and J. RAFELSKI: in *Hadronic Matter at Extreme Energy Density*, edited by N. CABIBBO and L. SERTORIO (Plenum Press, New York, N.Y., 1980), p. 49.
[10] A. CHODOS, R. L. JAFFE, K. JOHNSON, C. B. THORN and V. F. WEISSKOPF: *Phys. Rev. D*, **9**, 3471 (1974).
[11] J. KAPUSTA: *Nucl. Phys. B*, **196**, 1 (1982).
[12] J. BAACKE: *Acta Phys. Pol. B*, **8**, 625 (1977).
[13] N. CABIBBO and G. PARISI: *Phys. Lett. B*, **59**, 67 (1974).
[14] J. KAPUSTA: *Nucl. Phys. B*, **148**, 461 (1979).
[15] R. HAGEDORN and J. RANFT: *Suppl. Nuovo Cimento*, **6**, 169 (1968).
[16] Such models have been discussed by the author (p. 236) in *The Proceedings of the Workshop of Future Relativistic Heavy-Ion Experiments, Darmstadt, 1980*, GSI 81-6, Gesellschaft für Schwerionenforschung report GSI 81-6, Darmstadt, 1981.
[17] M. I. GORENSTEIN, V. P. SHELEST and G. M. ZINOVJEV: *Phys. Lett. B*, **60**, 283 (1976).
[18] E. L. FEINBERG: *Nuovo Cimento A*, **34**, 391 (1976).
[19] E. SHURYAK: *Phys. Lett. B*, **78**, 150 (1978).
[20] E. M. FRIEDLAENDER and R. M. WEINER: *Phys. Rev. Lett.*, **43**, 15 (1979).
[21] R. HAGEDORN: in *The Proceedings of the Workshop of Future Relativistic Heavy-Ion Experiments, Darmstadt, 1980*, GSI 81-6, Gesellschaft für Schwerionenforschung report GSI 81-6, Darmstadt, 1981, p. 267.
[22] L. D. LANDAU: *Collected Papers*, edited by D. TER HAAR (Pergamon Press, Oxford, 1965), p. 569.
[23] R. HAGEDORN: *Thermodynamics of strong interactions*, report CERN 71-12 (1971).
[24] K. IMAEDA: *Nuovo Cimento A*, **48**, 482 (1967).
[25] R. HAGEDORN and J. RAFELSKI: *Commun. Math. Phys.*, **83**, 563 (1982).
[26] UA5 COLLABORATION: *Phys. Lett. B*, **121**, 209 (1983).
[27] J. RAFELSKI and M. DANOS: *Phys. Lett. B*, **97**, 279 (1980).
[28] I. MONTVAY and J. ZIMANYI: *Nucl. Phys. A*, **316**, 490 (1979). For a simplified discussion, see also R. HAGEDORN: in *The Proceedings of the Workshop of Future Relativistic Heavy-Ion Experiments, Darmstadt, 1980*, GSI 81-6 ,Gesellschaft für Schwerionenforschung report GSI 81-6, Farmstadt, 1981, p. 269.
[29] L. VAN HOVE: *Phys. Lett. B*, **118**, 138 (1982).
[30] S. BARSHAY: *Phys. Lett. B*, **127**, 129 (1983).
[31] See ref. [3] and references given therein.
[32] E. V. SHURYAK: *Phys. Lett. B*, **107**, 103 (1981). For further information, see G. BAYM: in *Quark Matter Formation and Heavy-Ion Collisions, Proceedings of the Bielefeld Workshop, 1982* (World Scientific, Singapore, 1982), p. 17.
[33] *a*) T. ERICSON: *Nuovo Cimento*, **21**, 605 (1961); *b*) F. CERULUS: *Nuovo Cimento*, **22**, 958 (1961); *c*) H. SATZ: *Fortschr. Phys.*, **11**, 445 (1963); *d*) H. JOOS and H. SATZ: *Nuovo Cimento*, **34**, 619 (1964); *e*) K. ZALEWSKI: *Acta Phys. Pol.*, **28**, 933 (1965); *f*) A. KOTANSKI and K. ZALEWSKI: *Nuovo Cimento*, **40**, 134 (1965); *g*) C. B. CHIU and R. L. HEIMANN: *Phys. Rev. D*, **4**, 3184 (1971).

[34] R. HAGEDORN and U. WAMBACH: *Nucl. Phys. B*, **123**, 382 (1977).
[35] R. HAGEDORN: *Suppl. Nuovo Cimento*, **3**, 147 (1965).
[36] S. FRAUTSCHI and C. J. HAMER: *Phys. Rev. D*, **4**, 2125 (1971).
[37] R. HAGEDORN and I. MONTVAY: *Nucl. Phys. B*, **59**, 45 (1973).
[38] A. T. LAASANEN, C. EZELL, L. J. GUTAY, W. N. SCHREINER, P. SCHÜBELIN, L. VON LINDERN and F. TURKOT: *Phys. Rev. Lett.*, **38**, 1 (1977).
[39] G. W. VAN APELDOORN, S. BARSHAY, D. HARTING, D. J. HOLTHUIZEN, P. G. KUIJER, B. J. PIJLGROMS, V. KARIMÄKI, R. KINNUNEN, M. KORKEA-AHO, P. JOHNSON, P. MICHAELIDES, CH. MICHAELIDOU and D. G. PATEL: *Z. Phys. C*, **7**, 235 (1981).
[40] J. HOFMANN, W. SCHEID and W. GREINER: *Nuovo Cimento A*, **32**, 343 (1976).
[41] J. HOFMANN, B. MÜLLER and W. GREINER: *Phys. Lett. B*, **82**, 195 (1979).
[42] H. G. BAUMGARDT, J. U. SCHOTT, Y. SAKAMOTO, E. SCHOPPER, H. STÖCKER, J. HOFMANN, W. SCHEID and W. GREINER: *Z. Phys. A*, **273**, 359 (1975).
[43] H. STÖCHER, J. A. MARUHN and W. GREINER: *Phys. Rev. Lett.*, **44**, 725 (1980).
[44] R. HAGEDORN: in *The Proceedings of the Yorkshop of Future Relativistic Heavy-Ion Experiments, Darmstadt, 1980*, GSI 81-6, Gesellschaft für Schwerionenforschung report GSI 81-6, Darmstadt, 1981, p. 245.
[45] CERN-COLUMBIA-ROCKEFELLER COLLABORATION: *Phys. Lett. B*, **46**, 471 (1973).
[46] S. GEER (UA1) was the first to observe that the slope of the p_T tail of the UA1 measurement joins smoothly those of the ISR distributions and roughly obeys the law proposed in fig. 10 of ref. [16] (from which our fig. 4.1 was taken and UA1 data added). (Private communication from S. GEER.)
[47] UA1 COLLABORATION: *Phys. Lett. B*, **123**, 108 (1983).
[48] S. FRAUTSCHI: *Phys. Rev. D*, **3**, 2821; R. HAGEDORN and I. MONTVAY: *Nucl. Phys. B*, **59**, 45 (1973).
[49] R. HAGEDORN: *Relativistic Kinematics*, fifth printing (Addison-Wesley and Benjamin/Cummings Advanced Book Program, Reading, Mass., 1980).
[50] J. ERWIN, W. KO, R. L. LANDER, D. E. PELLETT and P. M. YAGER: *Phys. Rev. Lett.*, **27**, 1534 (1971).
[51] C. ANGELINI, L. BERTANZA, A. BIGI, R. CASALI, R. PAZZI, C. PETRI, E. ROMANI, C. DEFOIX, P. LADRON DE GUEVARA and P. PETITJEAN: *Lett. Nuovo Cimento*, **19**, 283 (1977).
[52] This is witnessed in low-$p_\perp$ measurements; see BRITISH-SCANDINAVIAN-MIT COLLABORATION: *Phys. Lett. B*, **64**, 111 (1976). See also P. CARLSON: *A note on* $\langle p_T \rangle$ *and the shape of the* p_T *spectrum for low values of* p_T, CERN/EP/SCE-R703T-UA5/P 83.8.

Direttore responsabile: RENATO ANGELO RICCI

Stampato in Bologna dalla Tipografia Compositori
coi tipi della Tipografia Monograf

Questo fascicolo è stato licenziato dai torchi il 10-X-1984

Questo periodico
è iscritto
all'Unione Stampa
Periodica Italiana